United States Department of Interior

Office of Surface Mining Reclamation and Enforcement

Applied Science Program

Backfill Geochemical Model and Treatments for Lessening Solute Mobility and Improving Aquifer Water Quality in Restored Coal Mine Pits, Powder River Basin

OSMRE: Idaho Backfill Aquifer Cooperative Agreement, S21AC10037

Final Technical Report

Jeff Langman, Associate Professor of Hydrogeochemistry, University of Idaho

Julianna Martin, M.S., University of Idaho

DISCLAIMER

ABSTRACT

Open-pit mining utilizes waste rock for landscape restoration during the post-mining period, which may include the construction of backfill aquifers. With the mining of the Powder River Basin coal deposits, waste rock is temporarily stored before landscape reconstruction, which includes the construction of backfill aquifers in the coal mine pits. With the reintroduction of groundwater to a backfill aquifer, weathering of the waste rock may release contaminants that were previously unavailable in the overburden/interburden material. Such changes to water quality are not easily predicted given the limited presence of such contaminants in groundwater found within the overburden material before mining. Impacts on water quality (regulatory criteria exceedance) from these new contaminant sources are highly variable, but such impacts have been documented for up to 15+ years in backfill aquifers of the Powder River Basin. The goal of this study was the characterization of the contaminant sources and weathering processes in backfill waste rock through benchtop weathering experiments, evaluation of newly available contaminant sources through geochemical modeling of waste rock weathering, and an evaluation of potential construction options for reducing contaminant transport in backfill aquifers.

Waste rock from the Cordero Rojo open-pit coal mine in the Powder River Basin was exposed to benchtop weathering experiments consisting of 4 kg leach columns saturated and drained twice a week for 20 weeks at temperatures of 5 °C and 20 °C. Column leachate was collected for analysis of Eh, pH, specific conductance, alkalinity, and cation and anion concentrations as unfiltered and 0.45-µm and 0.2-µm filtered concentrations. During the experiment, leachate Eh and pH substantially varied during the first 55 days, which corresponds to a period of high specific conductance and alkalinity values. Correspondingly, anion and cation concentrations were the largest during this early weathering stage and the filter fractions indicated multiple weathering processes, such as particle transport, salt dissolution, and sulfide oxidation. After this early weathering stage, all environmental parameters slowly evolved towards a chemical equilibrium of neutral, oxidizing, and low solute weathering conditions. This evolution was reflected in the decline and stabilization or non-detection of nonmetal and metal(loid) concentrations reflective of a shift to primarily bulk aluminosilicate weathering. Over the course of the experiment, the concentration trend of certain elements indicated particular weathering processes—cadmium and nanoparticle transport, selenium and salt dissolution, and arsenic and the oxidation of pyrite. Elements that are found in multiple mineral sources, such as iron, had concentration trends that indicated multiple weathering processes that occurred in the early weathering stage and throughout the experiment.

The mining of the overburden formations created newly available mineral surfaces and nanomaterials that could release elements into solution, which were not expected to be present, or in significant concentrations, given historical aquifer water quality for the overburden formations. To better predict the mobilization of high-priority contaminants, such as arsenic and selenium, basic forward geochemical models were constructed to replicate the typical modeling scenario for the identified mineral sources of arsenic and selenium in the Powder River Basin overburden—pyrite and gypsum, respectively. The basic forward models were unable to capture the arsenic and selenium concentration trends recorded for leachate from the 20 °C leach column. Enhanced models were constructed to capture nanomaterial contributions to supplement the initially identified processes of the oxidation of arsenic-bearing pyrite and dissolution of selenium-bearing gypsum. Incorporation of the nanomaterial contributions produced modeled arsenic and selenium

trends similar to what was observed in the column leachate. These modeling results indicate that the identification of additional contaminant sources for backfill waste rock is necessary to predict the exceedance of water quality criteria for overburden formations that have not previously shown the potential for water quality contamination. The presence of potential contaminant sources must be evaluated for greater weathering and release of the contaminants given the new mineral surfaces and available nanomaterials generated during the mining and reconstruction processes.

Additional 20 °C leach columns were amended through the introduction of soil, zeolite, compaction of the waste rock, and rinsing of the waste rock to evaluate available options for reducing contaminant transport because of the new mineral surfaces and nanomaterial issue. The amendments—soil, zeolite, compaction, and rinse—were considered possible treatments for the waste rock before or during the construction of the backfill aquifers. A soil layer is present in the overburden that could be separated during overburden removal and added as a layer-specific amendment during backfill. Similarly, zeolite is a readily available and low-cost soil amendment that has a long history of being used to reduce the transport of cationic solutes. Compaction was tested as a possible amendment with the consideration of enhanced construction techniques to increase compaction of the waste rock during landscape reconstruction to lessen available groundwater pathways that could interact with the newly available mineral surfaces and nanomaterials. The last amendment—rinsing—is a difficult treatment for the construction of backfill aquifers but was considered as a possible treatment if backfill aquifer construction was delayed and the temporarily stored waste rock exposed to greater surface weathering where runoff could be captured and treated. The leachate from the amended columns indicated that compacted and rinsed amendments were able to substantially reduce the release of solutes in comparison to the unamended leachate and the soil and zeolite amendments. The compaction amendment appears to restrict the flow of water, thereby restricting the interaction of water with the new contaminant sources in the waste rock. The rinse amendment provides for flushing of potential solutes before weathering of the waste rock and would require a change in storage of the waste rock before landscape reconstruction, including collection and treatment of runoff from surface storage of waste rock.

Table of Contents

Figures

Tables

Chapter 1. Introduction

1.1 Background

A backfill aquifer is produced from the filling of a mine pit with waste rock (e.g., overburden and interburden materials) and the return of groundwater from infiltrating precipitation and lateral inflow from the surrounding aquifer(s). As water percolates into the waste rock, a reaction front propagates through the aquifer as newly exposed mineral surfaces and small particles (e.g., nanoparticles) are exposed to weathering and transport processes (Jun et al., 2010; Sharma et al., 2015). Progression of the reaction front in weathering waste rock is visible in the temporal evolution of solute release until a new equilibrium of weathering is established (Acero et al., 2009; Blowes and Jambor, 1990; Dosseto et al., 2008; Yoo and Mudd, 2008). The difficulty in understanding the potential water quality of backfill aquifers is not our lack of mineral weathering knowledge, but our lack of understanding of the availability of potential contaminant sources contributing to solute release and transport in this modified aquifer matrix. The incomplete source identification for the prediction of solute release has resulted in the exceedance of water quality criteria for backfill aquifers when it was predicted that weathering of the waste rock would not result in groundwater contamination issues (Bartos and Ogle, 2002; Slagle et al., 1985). The purpose of this study was the identification and characterization of new contaminant sources that became available through the mining process and how we might reduce the potential water quality impacts of these contaminant sources.

Backfill aquifers in the Powder River Basin (Fig. 1), the largest coal mining district in the United States, have shown variable water quality and exceedance of water quality criteria for metal(loid) and nonmetal contaminants due to the weathering of waste rock used for landscape restoration. Reclamation of coal mines in the Powder River Basin has produced a range of water quality issues in backfill aquifers that have not been attributed to any particular waste rock characteristic or reclamation process (Reddy et al., 1995; Reed and Singh, 1986; Vance et al., 1998). The blasting and transport of the waste rock produce a new aquifer matrix with the generation of new mineral surfaces and nanomaterials that can produce high weathering and solute transport rates (Fig. 2) (Anderson et al., 2011; Colman, 1981; Dosseto et al., 2008; Drever and Clow, 1995; St-Arnault et al., 2020a). A weathering or release rate is the rate at which primary minerals are transformed into secondary minerals or dissolved reaction products, congruently or incongruently, with the release of elements/solutes (Colman, 1981). Predicting the release of solutes can be difficult because of coupled biogeochemical processes, but the identification of potential contaminant sources and associated reaction rates with the development of applicable conceptual and numerical models are critical for estimating solute release and evaluating future water quality (Futter et al., 2012; Malmström et al., 2000; Salmon and Malmström, 2006).

Our understanding of the chemistry, physics, and biology of weathering has advanced significantly through the examination of corrosive processes in the critical zone and regolith (Lebedeva and Brantley, 2020). A governing physical property of weathering is the available surface area where fine fractions typically undergo the greatest weathering that releases a substantial portion of the solutes (Banwart et al., 2002; Malmström and Banwart, 1997; Stockwell et al., 2006). The generation and transport of nanomaterials/nanoparticles (materials with at least one dimension within the nanometer scale (Hochella et al., 2008)) can contribute to the solute load through inclusion in dissolved phase (<0.45-μm filtering) and also will weather to produce additional solutes (Hochella et al., 2019). The complexity of predicting the quality of waste rock

drainage is often proportional to the scale of the studied waste rock (St-Arnault et al., 2020a). Therefore, complementary kinetic testing procedures, such as laboratory or field weathering experiments, are increasingly used to evaluate the weathering behavior of waste rock (St-Arnault et al., 2020b, 2019; Vriens et al., 2019b, 2019a). Using waste rock from the Cordero Rojo Mine in the Powder River Basin (PRB), a leach column experiment was conducted to discriminate solute sources from newly created mineral surfaces and transportable particles produced with the generation of the waste rock.

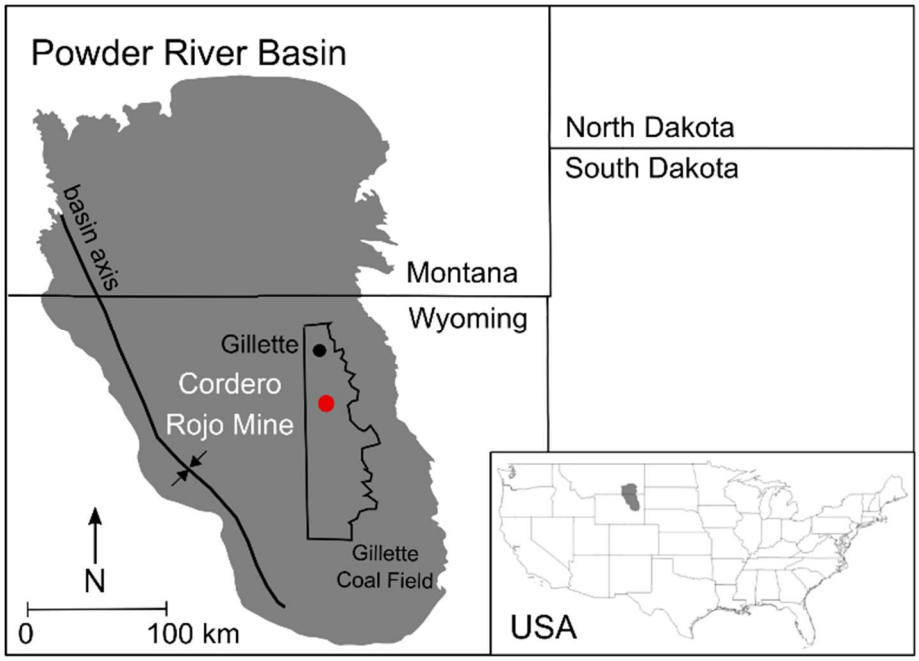

Figure 1. Location of the Cordero Rojo Mine in the Powder River Basin of Wyoming, USA.

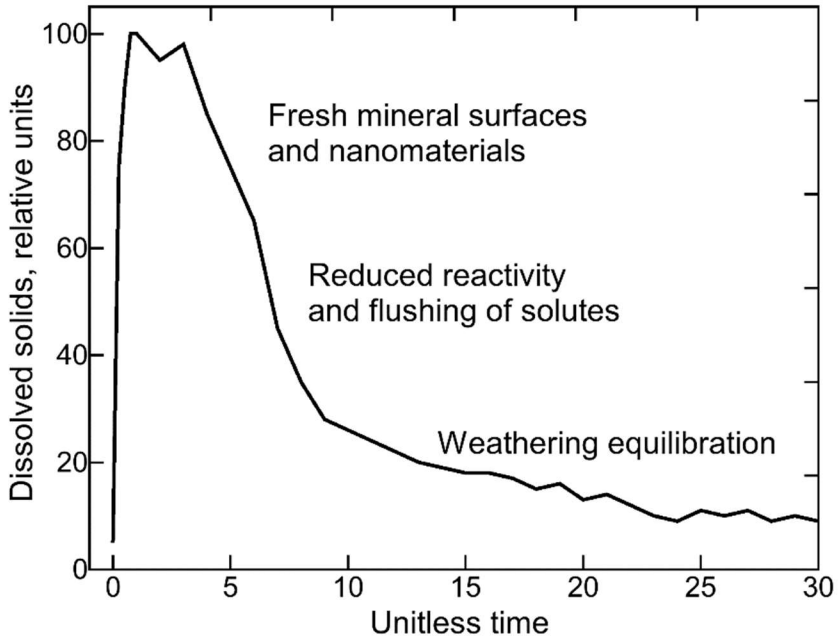

Figure 2. Typical trend of solute release with weathering of fresh waste rock (modified from Langman et al. (2014)).

1.2 Cordero Rojo Mine Geology

The PRB of Montana and Wyoming (Fig. 1) is a north-northwest to south-southeast trending asymmetric syncline. The basin contains greater than 5,500 m of sediments along the basin axis that sit atop Precambrian igneous and metamorphic rocks dipping gently westward from the Black Hills (Dolton et al., 1990). The structural axis is located along the western part of the basin with the western limb characterized by steeply dipping (~20º) strata and the eastern limb characterized by gently dipping (2–5º) strata, including the Cretaceous and Tertiary coal-bearing rocks (Flores, 2004). Because the coal beds are thick, shallow, and gently dipping along the eastern margin, large open-pit mines have been developed in this area to extract the coal. A typical mining operation of this region consists of overburden and coal removal with corresponding backfill moving westward (Fig. 3).

PRB waste rock is derived from sequences of interbedded fluvial, lacustrine, and palustrine deposits that compose the overburden/interburden of the Wasatch and Fort Union formations (Lorenz and Nadon, 2002; Pocknall, 1987; Yuretich et al., 1984). These formations contain an abundance of sandstone with some limestone and relatively non-sulfidic mudstones (primarily phyllosilicate clays such as smectite, vermiculite, kaolinite, illite, and chlorite) (Yuretich et al., 1984) whose paleoenvironments produced the low sulfur coal and very low sulfur waste rock (Ellis, 2002; McClurg, 1988; Moore, 1991). The PRB coal contains accessory minerals such as arsenic-bearing pyrite [FeS_2], cadmium-bearing sphalerite [(Zn,Fe)S], and galena [PbS] (Palmer et al., 1997). Primary contaminants (exceedance of water quality criteria) detected in PRB backfill aquifers include arsenic [As], barium [Ba], manganese [Mn], and selenium [Se] (Milligan and Reddy, 2007). Such contaminates typically are not found in groundwater that has interacted with the Wasatch and Fort Union formations (Wyoming State Engineer's Office, 1995). Therefore, it was hypothesized that production and disposal of the waste rock have incorporated small coal particles containing higher concentrations of the potential contaminants, exposed previously unavailable forms of the contaminants (e.g., bound salts), and/or produced contaminant-containing nanomaterials that are being weathered/transported within the backfill aquifers.

Figure 3. Example of the removal of overburden and waste generation during open-pit coal mining in a sedimentary basin, Cordero Rojo Mine, Powder River Basin, Wyoming, USA.

Chapter 2. Weathering Experiments

To evaluate the mobilization of contaminants and potential actions that could be taken to minimize their release and mobility, 4 kg leach columns were constructed with Cordero Rojo waste rock in warm-room (20 ºC) conditions. A duplicate cold-room (5 ºC) column was constructed for evaluating the temperature effect on waste rock weathering.

2.1 Evaluation of Possible Backfill Aquifer Construction Options

Amendments to backfill are not common for non-acid generating waste rock, but multiple options may be available for reducing solute transport during early weathering of PRB waste rock in backfill aquifer. Two low-cost amendments were evaluated for reducing contaminant transport in the waste rock—soil and zeolite. The topsoil from the field site was added to a leach column waste rock to form a mixed backfill layer to capture migrating solutes and nanoparticles. A soil replacement is an included part of landscape and ecological restoration for many mines and existing soils are often collected and stored onsite for use in the post-mining period (Fischer et al., 2022). A soil has the capacity to improve water quality through pH buffering, adsorption/desorption processes, and ion exchange as a result of the organic, mineral, and microbial components that makeup the soil (Adams et al., 2020; Cheng et al., 2021). A zeolite [hydrated $(Na,K,Ca)_{2\text{-}6}Al_xSi_yO_z$] amendment was incorporated into another leach column to take advantage of the microporous and sorbing nature of these aluminosilicate grains (Burakov et al., 2018; Pandová et al., 2018). Zeolites have the capacity to capture cationic solutes through sorption, can induce cation exchange of contaminants of concern, and are commonly referred to as "molecular sieves" because of their micropore structure that can retain captured metals (Holub et al., 2013; Motsi et al., 2009; Pandová et al., 2018; Stylianou et al., 2007; Wang and Peng, 2010).

In addition to the two added amendments (soil and zeolite) evaluated in the leach columns, two physical alteration amendments were evaluated for reducing solute transport—compact and rinsing. Compaction is a necessary part of reclamation required under the Surface Mining Control and Reclamation Act (SMCRA) to produce reclaimed land that resembles the approved post-mining contours. Land subsidence of coal mining areas has been a historical issue, particularly with underground mines in weak overburden areas (Dunrud and Osterwald, 1978; Karfakis and Topuz, 1991). Compaction decreases subsidence/settling and is an important stabilizing process during construction of backfill aquifers that can influence the aquifer's porosity/permeability and hydraulic pathways (Doulati Ardejani et al., 2003; Naderian et al., 1996; Sun et al., 2017; Zhang et al., 2019). By reducing permeability and available pathways in backfill aquifers, the newly available contaminant sources may be restricted from weathering or release solutes may have limited available flowpaths, which would lessen potential water quality impacts. Given that compaction occurs during backfill through fill and grading operations, we compared the loose settling (no compaction) of waste rock in the primary-warm-room column to a compacted (10% volume reduction), warm-room column. The last amendment, rinsing, is a difficult treatment for construction of backfill aquifers but was considered as a possible treatment if backfill construction is delayed, exposing the waste rock to longer surface weathering where runoff could be captured and treated. Such a change in landscape reconstruction may be possible with delayed backfilling, but the capture of water passing through the surface-stored waste rock and mobilizing early contaminants may be difficult.

2.1 Waste Rock Sampling

Waste rock samples of the Wasatch and Fort Union formations were collected within 2 weeks of initial excavation from the Navajo Transitional Energy Company's Cordero Rojo Mine in the Powder River Basin. Sample collection was completed according to the "clean hands" techniques as prescribed for field and laboratory experiments involving trace metals (Environmental Protection Agency, 1996; United States Geological Survey, 2006). The Wasatch and Fort Union waste rock were collected separately (the two types are segregated during mining) through a random selection method per standard practice for sampling aggregates (American Society for Testing and Materials, 2016) and screened to ≤ 6.3 mm (standard sample size for kinetic/humidity columns) in the field (Fig. 4) (American Society for Testing and Materials, 2018a; Lapakko, 2003; Lapakko and White, 2000). The 300 kg of screened waste rock (86 kg Wasatch waste rock and 214 kg Fort Union waste rock) was sealed in 0.02 m^3 buckets and transported to the University of Idaho where the waste rock was temporarily stored at 5 °C until dried at 125 °C for 48 hours. Subsamples of the dried waste rock were collected for element composition, mineral identification, grain size distribution analysis, slake durability, and mean surface area.

Figure 4. Cordero Rojo Mine waste rock samples being sieved to ≤ 6.3 mm onsite.

2.2 Leach Column Construction

The leach columns consisted of a 0.6-m length, 0.1-m diameter, clear PVC (Fig. 5). Each column was sealed with rounded endcaps, and the top cap contained a 0.5-cm open hole for escaping air during water introduction. The bottom endcaps contain two-layered mesh filters for the retention of the waste rock material. These mesh filters contain sufficiently large diameter openings to allow ≤ 10-µm particles into the upper mesh and a restriction to ≤ 4-µm particles in the lower mesh prior to discharge through 1-cm tubing into leachate collection containers. Leachate trials were conducted to evaluate the ability of the mesh filters to reduce particle size of leachate to an acceptable limit and to ensure retention of the material in the column. The goal was

to allow possible solutes to pass the mesh filter that mimics the transport of solutes (micron-to-nanometer in scale) in a backfill aquifer. Additionally, the mesh filters had to remain open for leachate flow (no clogging) over the lifespan of the experiments (e.g., months). Lastly, the mesh filters allowed for sufficient flow rates for the total leachate volume to be collected in a reasonable amount of time.

Warm-room (20 °C ± 1 °C) and cold-room (5 °C ± 0.5 °C) PVC columns (0.6 m (H) × 0.1 m (W)) were loaded with 0.8 kg of Wasatch waste rock and 3.2 kg Fort Union waste rock (Table 1) to mimic overburden distributions at the Cordero Rojo Mine, which is replicated with backfill aquifer construction. The compaction column consisted of a column sample compacted to 90% of a loose pour volume through agitation and hydraulic press for comparison to the no compaction columns. For amendments of soil and zeolite, the Fort Union waste rock and amendment were homogenized (American Society for Testing and Materials, 2016). No modifications were made to the soil to preserve soil properties generated onsite at the Cordero Rojo Mine. A specific zeolite mineral, clinoptilolite [$(Na,K,Ca)_{2\text{-}3}Al_3(Al,Si)_2Si_{13}O_{36}\cdot 12H_2O$], was obtained from KMI Zeolite, Inc. (Nevada). The clinoptilolite had a diameter range of 2.4 to 4.8 mm (4 × 8 mesh, median of 3.5 mm) and an approximate surface area of 40 m^2/g (manufacturer determined). This type of zeolite has a 10- and 8-ring (framework element) micropore structure, which is considered a larger ring size in the zeolite family (Baerlocher et al., 2007). To reduce a possible initial influence on solute concentrations, clinoptilolite grains were triple-rinsed with reverse-osmosis filtered water (ultrapure water) and dried at 80 ºC to remove clinoptilolite nanomaterials generated during mining and handling. The rinsed amendment consisted of a triple rinse of the waste rock load with ultrapure water. The cold-room column was a duplicate of the unamended warm-room column to allow for evaluation of the temperature effect on waste rock weathering.

Table 1. Column identification codes and associated amendments.

Column Code	Temperature	Amendment
1W	20 ºC ± 1 °C	None, warm-room standard
2ZW	20 ºC ± 1 °C	Zeolite
3SW	20 ºC ± 1 °C	Soil
4CW	20 ºC ± 1 °C	Compaction
5RW	20 ºC ± 1 °C	Rinsed
6C	5 ºC ± 0.5 °C	None, cold-room standard

2.3 Weathering Procedures and Leachate Testing

The weathering cycle for each leach column consisted of a semiweekly schedule of the drip introduction of 1-L of deionized water and full saturation of the 0.6-m column of waste rock for 72 hours followed by a 2-hour drain period and a 6-hour unsaturated period before re-saturation of the column. This is a modification of the standard humidity cell protocol (American Society for Testing and Materials, 2018b) to simulate primarily saturated (e.g., aquifer) conditions and allow for the collection of sufficient water volume for analysis of field parameters and solutes. The twice-weekly leachate from each column was analyzed for pH (± 0.01 pH), Eh (± 0.2 mV), and specific conductance (± 0.01 µS/cm) with calibrated Orion 3-Star meters/probes. Alkalinity (± 0.1 mg/L as $CaCO_3$) was determined by an OrionStarT940 auto titrator using 0.1 N HCl. Anion (bromide [Br], chloride [Cl], fluoride [Fl], nitrate-nitrite as nitrogen [NO_3-NO_2 as N], ortho-phosphate [PO_4], and sulfate [SO_4]) concentrations were determined by ion chromatography (Dionex Aquion Ion Chromatograph) from 0.45-µm filtered leachate. Cation (aluminum [Al], arsenic [As], barium

[Ba], boron [B], cadmium [Cd], calcium [Ca], chromium [Cr], copper [Cu], iron [Fe], lead [Pb], magnesium [Mg], manganese [Mn], molybdenum [Mo], nickel [Ni], potassium [K], selenium [Se], sodium [Na], zinc [Zn]) concentrations of unfiltered and filtered (0.45-µm filtered and 0.2-µm filtered) leachate were determined by inductively coupled plasma optical emission spectrometry (ICP-OES) for larger concentrations (Perkin Elmer Optima 8300 ICP-OES) and inductively coupled plasma mass spectrometry (ICP-MS) for smaller concentrations (Agilent 7800 ICP-MS) at the University of Idaho Analytical Services Laboratory. Duplicate samples were randomly collected during each leachate collection to assess analysis accuracy over the 20-week experiment period.

Figure 5. Constructed and filled leach columns for benchtop experiments conducted with Cordero Rojo Mine waste rock.

Chapter 3. Waste Rock Physical and Chemical Characterization

3.1 Physical Characterization

Grain size analyses conducted at the University of Idaho for Fort Union and Wasatch waste rock display a distribution reflective of their respective depositional environment. Fort Union waste rock indicated a greater percentage of fine (< 0.15 mm) grains indicative of its low energy depositional environment, as well as a larger percent of coarse (> 2 mm) coal grains incorporated from the blasting. Comparatively, Wasatch Formation waste rock primarily ranged from 4.75 mm to 0.3 mm. Grain size analyses of post-experiment waste rock (location sampled as compared to formation-specific) indicated more narrowly distributed grain sizes (0.04 mm to 2 mm) than the pre-experiment waste rocks indicative of the loss (e.g., transport, weathering) of small particles (Fig. 6). Post-experiment waste rock from the middle and top of the weathering column have an even narrower distribution than the lower column sample.

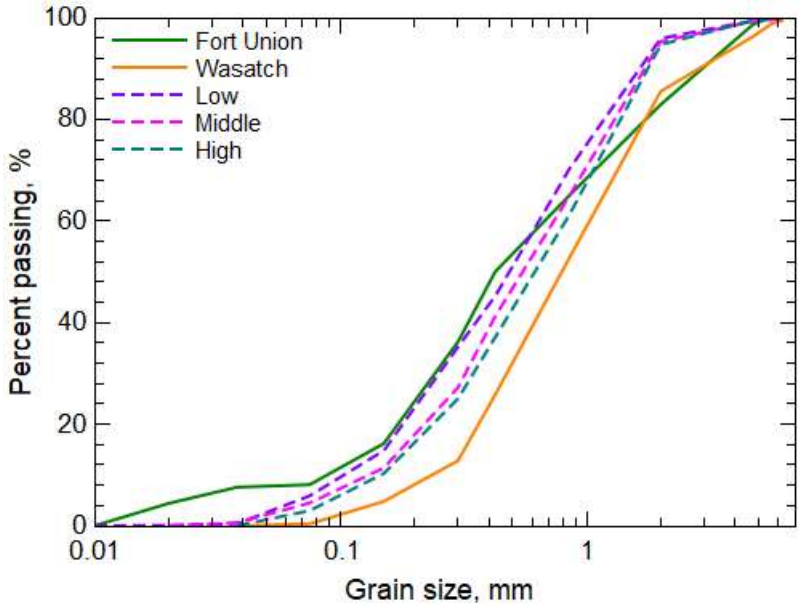

Figure 6. Grain size analysis of waste rock from the Fort Union and Wasatch formations and post-experiment waste rock sampled at three locations within the leach column (low, middle, and high).

Results from the slake durability tests conducted at the University of Idaho (American Society for Testing and Materials., 2004) indicated stronger rock (93 % durability index) for Wasatch waste rock compared to the durability index of 89 % for Fort Union waste rock. Such results align with the presence of substantial sandstone in the Wasatch Formation compared to the higher content of mudstones in the Fort Union Formation. The greater presence of smaller particles in the Fort Union waste rock (Fig. 6) translated to a much greater surface area of 14.2 m^2/g for the Fort Union sample compared to the 5.1 m^2/g determined for Wasatch waste rock.

3.2 Chemical Characterization

X-Ray fluorescence (XRF) analysis (Washington State University, Hooper Laboratory, Advant'XP+ sequential XRF with fused beads) indicated large concentrations of Al and silicon [Si] were present in the Wasatch and Fort Union waste rock reflective of the dominant

aluminosilicate minerals that compose these fluvial and lacustrine deposits (Dolton et al., 1990; Roehler, 1987) (Fig. 7). Larger accumulations of redox-sensitive elements of Fe, Mn, and P were present in the Fort Union waste rock, which are indicative of the low-energy depositional environments associated with certain units of the Fort Union Formation (Ayers, 1986; Hagmaier, 1971). Results from XRF analysis of the two types of waste rock indicated 7 ppm of As in the Fort Union sample and 2 ppm in the Wasatch sample (Se was not part of the XRF analysis package).

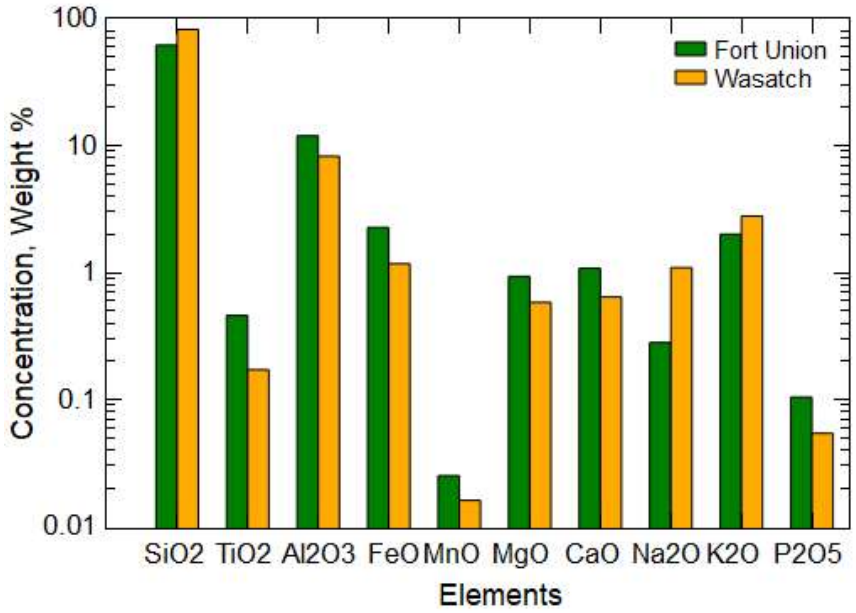

Figure 7. Element composition of the Fort Union and Wasatch waste rock from the Cordero Rojo Mine.

Random samples of ≤ 6.3 mm Fort Union and Wasatch waste rock were examined at the University of Idaho Electron Microscopy Center with a scanning electron microscope (Zeiss Supra 35 Variable-Pressure FEG SEM with Noran System Six EDS) to identify potential sources of As and Se that were selected for geochemical modeling. Given the expectation of As association with coal particles incorporated into the waste rock during overburden removal, an additional Fort Union sample was screened for coal particles by flotation for SEM analysis. For this flotation separation, 75 g of Fort Union waste rock was placed in a 1-L beaker with 500 mL of deionized water and agitated with an orbital shaker for 2 hr. Approximately 2 g of coal particles floated to the water surface and were collected and inserted into a lypholizer for 24 hr.

Examination of the ≤ 6.3 mm Wasatch and Fort Union waste rock with the SEM-EDS indicated the presence of As in coal particles (Fort Union sample) and distributed concentrations of Se (~0.2 wt %) in areas with high clay content (Fort Union and Wasatch samples). Analysis of separated (floated) coal particles from the Fort Union sample indicated that As was consistently present in trace amounts (0.1 to 0.6 wt %) throughout the coal particles. In the separated coal particle sample, Se was detected (up to 6.7 wt %) in clay particles absorbed to the larger particle surfaces (primarily coal). Results suggest a coal source for As and sorbed or precipitated Se particles (e.g., salts).

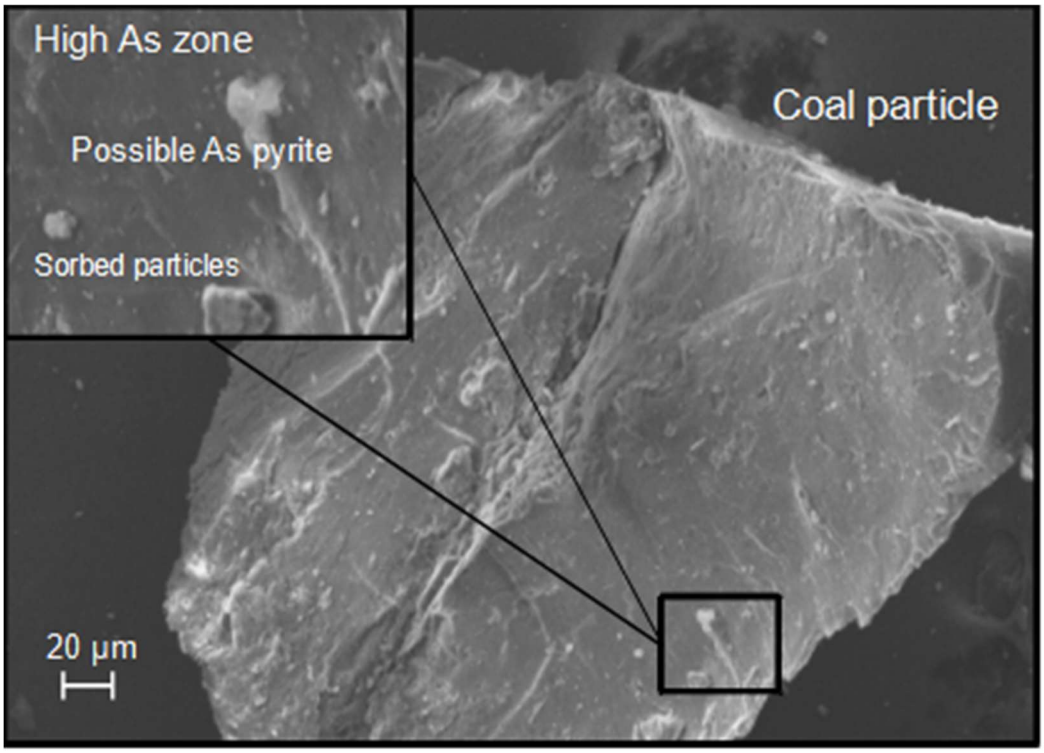

Figure 8. The identifiable presence of arsenic as arsenic-bearing pyrite and sorbed particles on a pre-experiment, coal particle screened from the Fort Union waste rock.

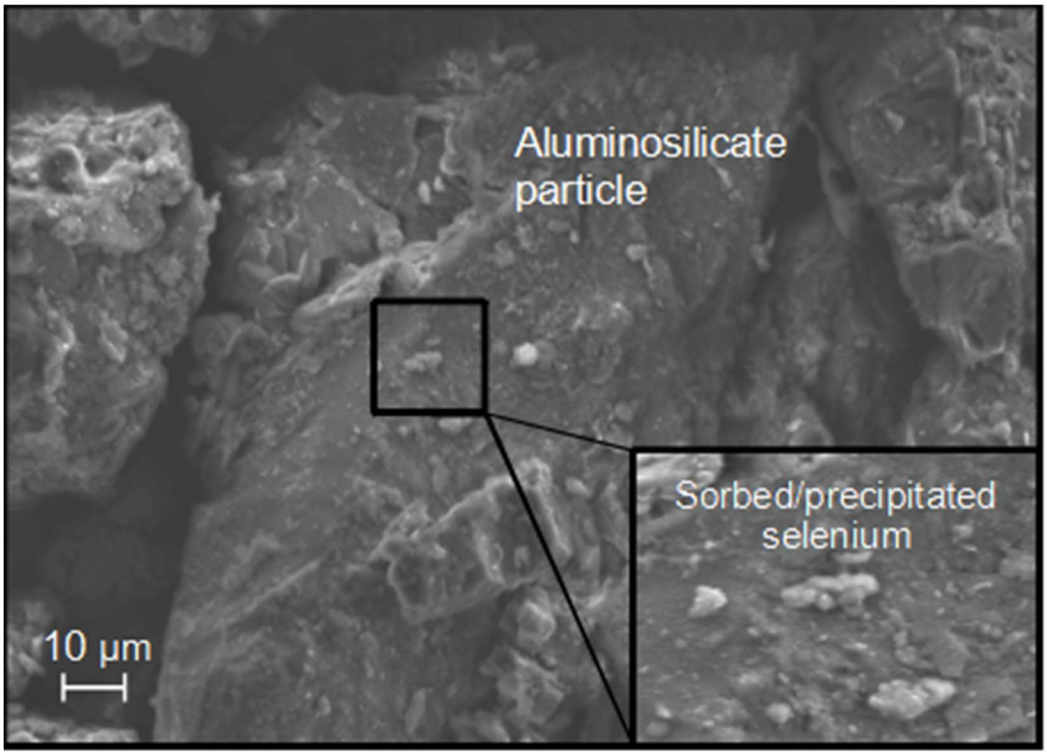

Figure 9. The identifiable presence of a sorbed selenium (e.g., selenite [SeO_3]) on pre-experimental plagioclase particle in the Fort Union waste rock.

Chapter 4. Weathering Column Leachate Analysis

4.1 Field Parameters

The environmental conditions for unamended warm- and cold-room leachate indicated high variability during the first 55 days of the experiment (Fig. 10). Eh fluctuated between positive values (maximum of 142 mV for warm-room leachate and 154 mV for cold-room leachate) and negative values (minimum of −113 mV for the warm-room leachate and −118 mV for the cold-room leachate) indicating alternating oxidizing and reducing conditions with the greatest variability during the first 45 days (Fig. 10a). Specific conductance ranged from 6,410 µS/cm to 315 µS/cm for the warm-room leachate and 6,350 µS/cm to 271 µS/cm for cold-room leachate, and the specific conductance of leachate from both unamended columns decreased sharply during the first 40 days of the experiment (Fig. 10b). Values of pH remained near neutral for the entire experiment, ranging from 6.05 to 7.03 for the warm-room leachate and 6.47 to 7.04 for the cold-room leachate (Fig. 10c) but indicated a greater temperature difference in pH values during the first 55 days. Alkalinity ranged from 550 mg/L to 148.3 mg/L for the unamended, warm-room leachate and 613 mg/L to 139 mg/L for the cold-room leachate (Fig. 10d) with a sharp decline during the first 20 days and a slower decrease from Day 20 to Day 70. Leachate Eh trends for amended and unamended were similar throughout the experiment (Fig. 10a). The zeolite-amended leachate had the highest pH and alkalinity throughout the experiment while the unamended, warm-room column contained leachate with the lowest initial pH. The soil-amended leachate displayed a period of high specific conductance from Day 23 until Day 90, diverging from the specific conductance trends observed in the other columns, indicating a potentially longer duration of flushing of solutes (e.g., nanoparticles), contributed by the soil amendment.

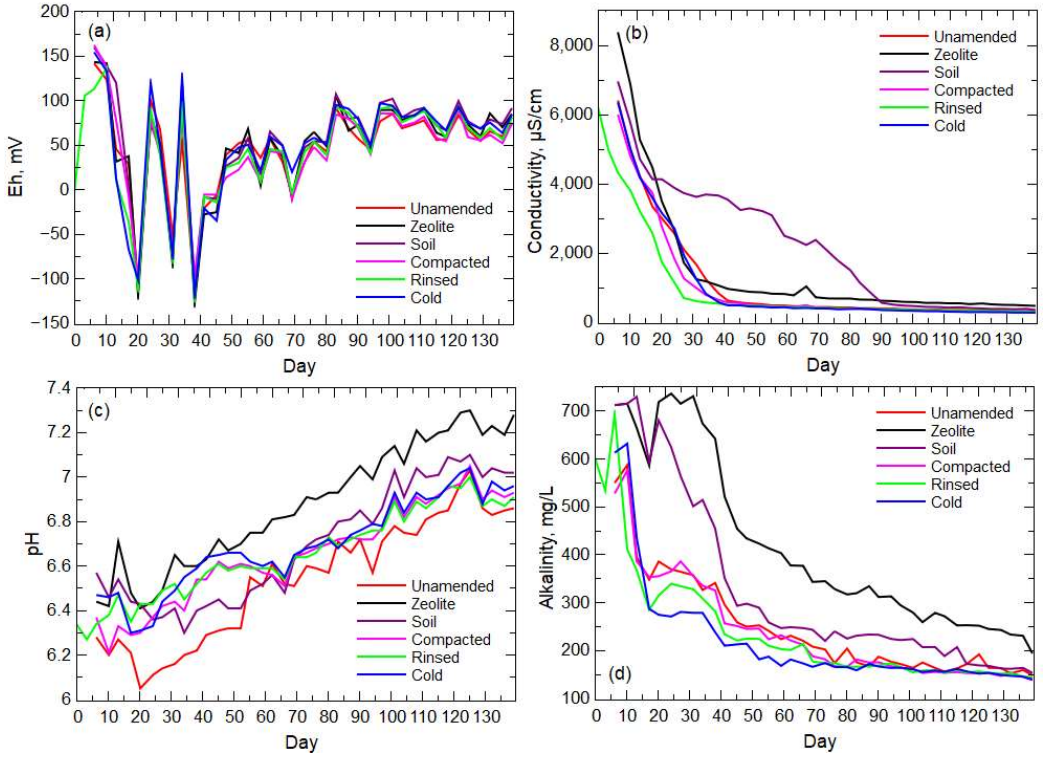

Figure 10. The field parameter results for (a) Eh, (b) specific conductance, (c) pH, and (d) alkalinity of leachate for unamended and amended columns.

4.2 Environmental Condition and Solute Trend Analysis

The goal of the leachate data analysis was the evaluation of the temporal trends, or variability with time, of the environmental conditions and release of solutes for the identification of substantive changes in weathering processes. The temporal trends of the environmental conditions of specific conductance, pH, and alkalinity were smoothed using the moving window average (4-point window) technique to reduce the volatility of the data series and allow for an improved display of the data trends. Values of Eh were not smoothed to preserve reduction-oxidation (redox) conditions that widely varied during the experiment. A principal component analysis (PCA) was used to identify clusters of related metal(loid) solutes for discriminating potential weathering processes in warm and cold conditions and the unfiltered and filter fractions. Solute data sets that were predominantly (> 80 %) below laboratory reporting limits were not included in the PCA.

The first component (PC1, Table 2) of the PCA indicated an association (covariance of 0.14) of the major cations (Ca, Mg, and K) along with Mn, Ni, and Zn that is consistent in the total and filtered concentrations in unamended warm- and cold-room conditions (Table 1, blue bold values). This association of the major ions in unfiltered and filtered samples indicates primarily bulk aluminosilicate and carbonate weathering throughout the experiment. The inclusion of Mn and Zn in this associated group likely reflects the presence of Mn and Zn-bearing carbonate species (Palmer et al., 2001). Additionally, Ni likely is associated in an insoluble form or possible clay source (Finkelman, 1987; Finkelman et al., 2018; Palmer et al., 2001). The association of the redox-sensitive Mn with elements released from aluminosilicate and carbonate minerals is supported by the lack of correlation (Spearman ρ of −0.04 to −0.03) between unamended Eh and Mn concentrations (unfiltered or filtered), where a correlation would be expected if the Mn was being released with sulfide oxidation. The second component (PC2, Table 2) of the PCA indicated a correlation of As and filtered Fe concentrations likely because of their association in sulfide minerals (e.g., As-bearing pyrite) that can be found in the coal (Ellis, 2002; Finkelman et al., 2018). The second component of the PCA also indicated an opposing correlation of Mo (positive) and Fe and As (negative) in the unamended, warm-room leachate (lack of detectable concentrations in the cold-room leachate), which may be indicative of the presence of Mo in the coal (Frascoli and Hudson-Edwards, 2018), but from a different mineral source than Fe and As. The association of Mo in PC2 is derived from a sulfide source, which is supported by a strong, positive correlation (Spearman's ρ of 0.58 to 0.55) between Mo and Eh. Prior analysis of PRB coal has indicated an average Mo concentration of 1.5 ppb (Peabody Energy, 2022), and the expected mineral occurrence for Mo is molybdenite [MoS_2] (Greber et al., 2015; Wang et al., 1994). The difference in association between Mo and other redox-sensitive elements may be due to the limited effects of pH on molybdenite dissolution (Johnson et al., 2019) and wide range of redox species (Chappaz et al., 2018).

Table 2. The covariance matrix of the principal component analysis for unamended, warm- and cold-room solute concentrations for each concentration fraction (total (unfiltered), 0.45-µm filtered, and 0.2-µm filtered). Associations identified through bold and colored (red for negative, blue for positive) fonts.

Element		Warm-room condition			Cold-room condition		
		Total	**0.45-µm**	**0.2-µm**	**Total**	**0.45-µm**	**0.2-µm**
As	PC1	0.02	0.03	0.03	0.09	0.13	0.13
	PC2	**-0.29**	**-0.26**	**-0.27**	-0.09	0.12	0.13
Ba	PC1	-0.13	-0.13	-0.13	-0.12	-0.13	-0.13
	PC2	0.09	0.09	0.09	0.14	0.14	0.14
B	PC1	0.11	0.14	0.14	0.09	0.14	0.14
	PC2	-0.05	0.01	0.01	0.06	-0.05	-0.05
Ca	PC1	**0.15**	**0.15**	**0.15**	**0.14**	**0.14**	**0.14**
	PC2	0.01	0.01	0.01	-0.03	-0.02	-0.02
Fe	PC1	0.11	0.06	0.07	0.03	-0.06	-0.06
	PC2	**-0.12**	**-0.27**	**-0.26**	0.14	-0.01	-0.01
Mg	PC1	**0.14**	**0.14**	**0.14**	**0.14**	**0.14**	**0.14**
	PC2	0.07	0.07	0.07	0.05	0.05	0.05
Mn	PC1	**0.14**	**0.14**	**0.14**	**0.14**	**0.14**	**0.14**
	PC2	-0.07	-0.07	-0.06	-0.04	-0.01	-0.01
Mo	PC1	-0.02	-0.02	-0.01	0.03	0.03	0.03
	PC2	0.26	0.25	0.27	0.23	0.26	0.26
Ni	PC1	**0.14**	**0.14**	**0.14**	**0.14**	**0.14**	**0.14**
	PC2	0.04	0.05	0.05	0.07	0.08	0.08
K	PC1	**0.14**	**0.14**	**0.14**	**0.14**	**0.14**	**0.14**
	PC2	0.04	0.05	0.05	0.03	0.03	0.03
Zn	PC1	**0.14**	**0.14**	**0.14**	**0.14**	**0.14**	**0.14**
	PC2	0.06	0.04	0.06	0.05	0.04	0.04

4.3 Salt Dissolution or Nanomaterial Weathering

The PCA did not include elements such as Cd and Se that were only detectable in the leachate during the first two weeks of the experiment (Fig. 11a,b). These elements have an association with sulfide minerals in the PRB coal (Bao et al., 2022; Kolker et al., 2002; Ya. E. Yudovich and Ketris, 2006), but their concentration trends did not mimic a release with the oxidative dissolution of pyrite that is visible with the As concentrations (Fig. 11c). In the waste rock formations, Se can be found in the coal, coal-associated pyrite, water-leachable salts, and as sorbed particles (e.g., selenite [SeO_3]) (Ya. E. Yudovich and Ketris, 2006). Dreher and Finkelman (1992) indicated that Se salts from past oxidation of pyrite may be the primary source of Se in the overburden, although they found seven different forms of Se with no discrimination between Wasatch and Fort Union formations. The quick release of Se and lack of difference within filter fraction concentrations and between temperature conditions are indicative of a fast-dissolving salt and/or desorption and oxidation of Se particles, such as selenite. The incorporation of Se into gypsum [$CaSO_4$] can occur with the oxidation of pyrite/coal and the substitution of Se for S in gypsum (Stillings, 2017; Wang et al., 2021). Such processes are partially responsible for the significant presence of gypsum in Powder River Basin sedimentary formations (Healy et al., 2008; Huggins et al., 1983; Lee, 1980; Rice et al., 2008; See et al., 1995). Se-bearing salts can readily dissolve, but the dissolution of the salts may not contribute substantial soluble Se species (e.g., selenate [SeO_4^{2-}]) if selenite is produced given the preference of selenite to readily sorb to sediments (Elrashidi et al., 1987; Paydary et al., 2021; Torres et al., 2018). The Se release from the leach column appears to be influenced both by particle release (early and large concentrations) with contributions from Se salt dissolution that is more visible in the second week when the warm-room leachate indicated higher concentrations of Se.

The Cd trend in the leachate indicates an early concentration peak that quickly decreased below reporting limits after Day 3 for all filtered warm- and cold-room results, and after Day 7 for total (unfiltered) warm-room leachate (Fig. 11a). Cadmium has not been documented as a salt byproduct from the oxidation of sulfide minerals in the Fort Union Formation, but Cd is associated with sphalerite [(Fe,Zn)S] found in PRB coal (Finkelman et al., 2018). Given the presence of Se salts from the oxidation of pyrite, it can be assumed that Cd was similarly released with sphalerite oxidation and deposited in the overburden formations. The introduction of leach water to the waste rock would not have a similar mobilizing effect on Cd compared to Se if both elements are contained in readily dissolvable salts since Cd is less soluble than Se (Stoeppler, 1992). This lower solubility of Cd is reflected in the much lower concentrations of Cd released from the waste rock compared to Se (Fig. 11b) even though there are equivalent amounts of Cd and Se in the coal seam (Brownfield et al., 2005). With the lower solubility of Cd, it is assumed that the release of Cd from the waste rock early in the experiment is because of the transport of Cd-bearing particles. Not all of the Cd was present in nanoparticles given the greater release of Cd in the unfiltered warm-room leachate, which indicated a more tortured path of the release of larger particles being transported from the waste rock. Comparison of the pre-experiment Wasatch and Fort Union samples to post-experiment waste rock from the warm-room, leach column indicated the loss of the smallest grains

(< 0.07 mm) from the Fort Union sample pre-experiment waste rock indicative of the loss (e.g., transport, weathering) of small particles (Fig. 6).

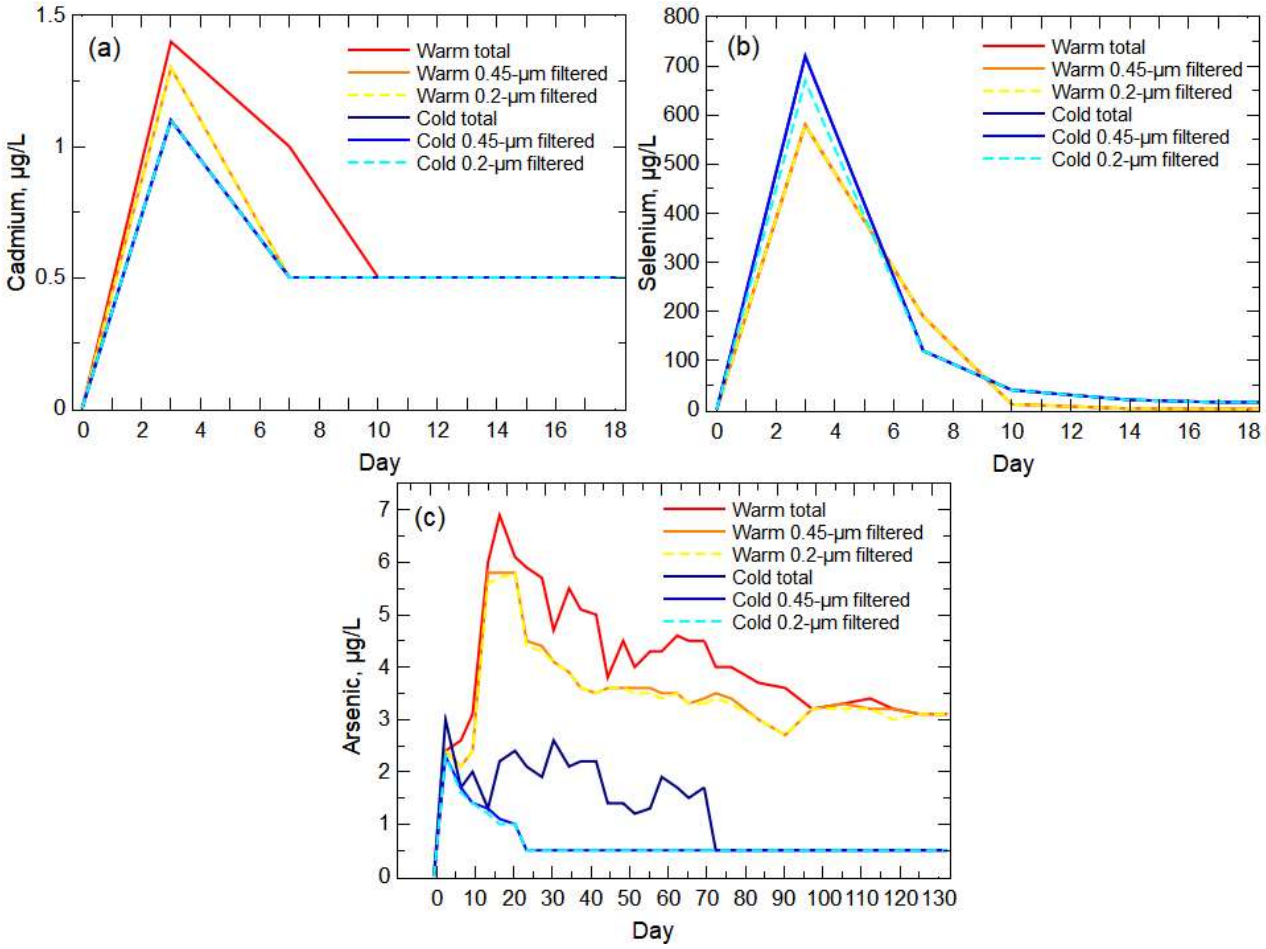

Figure 11. Unfiltered (total) and filtered concentrations in the unamended, warm-room and cold-room leachate for (a) cadmium and (b) selenium during the first 18 days of the experiment and (c) arsenic during the entire length of the experiment. All non-detect values were set to 0.5 µg/L, which is half the reporting limit for each of the analytes.

4.4 Oxidation Reactions

A Spearman rank correlation analysis of Eh and redox-sensitive elements (As, Fe, Mn, Mo) was performed to identify elements that may reflect the oxidative dissolution of sulfide minerals, such as pyrite, that are present in the Fort Union Formation (Palmer et al., 1997). The Spearman test is a nonparametric measure of rank correlation (statistical dependence between the rankings of two variables) that produces a statistic (ρ) that ranges between +1 (perfect positive relation) and −1 (perfect negative relation). This correlation analysis was performed using unamended, warm-room, unfiltered and filtered values due to substantial non-detection values for these elements in the cold-room leachate. Additionally, the activation energy (E_a, Eq. 1) of the oxidative dissolution of pyrite was calculated to evaluate temporal changes in pyrite weathering that may indicate inhibition of sulfide weathering because of precipitate formation (Fan et al., 2022). Arsenic was

selected for the calculation of the activation energy because of its strong correlation with Eh and the presence of Fe and sulfur [S] in other mineral sources found in the waste rock (Kolker et al., 2002). The Arrhenius equation using a single temperature and rate constant (Eq. 1) was used to calculate E_a instead of the typical two-temperature/two-rate constant method because cold-room As concentrations decreased below detection levels during the experiment. The one temperature/rate constant method employs the geometric solution or slope (line of best fit) of the ln(k)-to-time relation for estimating E_a:

$$\ln(k) = \ln(\mathrm{A}) - \left(\frac{\mathrm{Ea}}{\mathrm{RT}}\right) \qquad \text{Eq. 1}$$

where E_a is the activation energy ($J \cdot mol^{-1}$), R is the universal gas constant (8.314×10^{-3} $J \cdot mol^{-1} \cdot K^{-1}$), A is a pre-exponential factor (s^{-1}), and T is the temperature (K) at the respective times of the observed rate constants (k in $mol \cdot m^{-2} \cdot s^{-1}$).

Arsenic concentrations were largest in unamended, warm-room and cold-room leachate during the early weathering stage when Eh varied between positive and negative values (Fig. 11c) reflective of the likely consumption of oxygen with sulfide mineral weathering. The correlation analysis also indicated a strong to moderate negative correlation (Spearman's ρ of −0.56 to −0.29) between As and Eh. The majority of the As released in the warm-room leachate was present in the 0.2-µm filtered samples indicating ion release and/or small nanoparticles. The unfiltered leachate from both temperature conditions indicated additional As release in microparticles being transported from the columns. The release of an element such as As with pyrite weathering typically would result in an initial peak concentration because of the dissolution of an outer layer (rim or coating) followed by a moderated release according to the mass-to-volume ratio of the available mineral source (Acero et al., 2007). The primary loss of As from the waste rock is in the filtered fractions with a trend that peaks near Day 17 followed by a moderate decrease. The post-peak release of As is indicative of weathering of the As-bearing pyrite contained in the PRB coal that was incorporated into the waste rock. Such a trend follows the expected element release with the oxidative dissolution of pyrite (Williamson and Rimstidt, 1994a).

Calculation of the activation energy of pyrite weathering (Fig. 12) presents a typical energy trend of an initial energy barrier (oxidation of the mineral surface), an early drop in energy barrier as the sulfide surface degrades, and a slow increase in the necessary energy for oxidation of the remaining sulfide mineral. This trend represents the oxidation of the unreacted sulfide surface (shrinking core model) that becomes controlled by the inward diffusion of oxygen given the pore-blocking effect of Fe and S precipitates on the unreacted sulfide surface (Hu et al., 2006). This oxygen diffusion effect is more pronounced in neutral conditions where Fe is not solubilized and can form substantial Fe (oxyhydr)oxides with the eventual loss of the S intermediaries (Langman et al., 2015; Wunderly et al., 1996). The activation energy trend aligns with the evolution of activation energy necessary for the different bonding arrangements where the initial dissociation of oxygen at the sulfide surface required an activation energy of 22.6 kJ/mol (Dos Santos et al.,

2016) (compared to our calculated 18.2 kJ/mol) followed by lower energy requirements with degradation of the mineral structure.

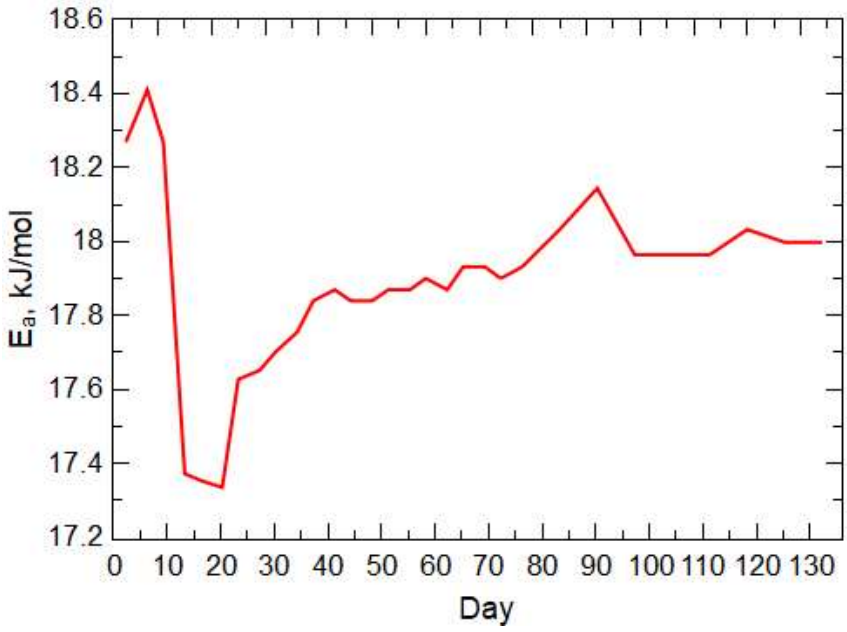

Figure 12. Activation energy (E_a) of pyrite weathering derived from unamended, warm-room leachate arsenic concentrations during the 20-week experiment.

4.5 Bulk Solid Weathering

With the identification of salt dissolution, particle transport, and pyrite oxidation contributing to the high solute release period, an additional weathering process is necessary to explain the large concentrations in all solutes during the early weathering stage and the following period of higher alkalinity. Transport of other particle types and weathering of the bulk aluminosilicate and carbonate minerals likely explains the remaining contributions to the high solute and high alkalinity periods prior to the waste rock equilibrating to the low solute weathering period (post-Day 70). Carbonates typically weather at a higher rate compared to aluminosilicates (Lehmann et al., 2022), which may explain the higher Ca concentrations compared to K (Fig. 13a,b) even though there is greater K present in the Wasatch and Fort Union waste rock (Fig. 7). Carbonate weathering likely is responsible for the pH moderation and increase during the experiment (Fig. 10), as well as the longer period of high alkalinity compared to the specific conductance period. The large, early concentrations in each of these element's concentration trends suggest release of Ca- and K-bearing nanoparticles (Hochella et al., 2019), desorption (exchangeable ions) from larger particles (Agbenin and van Raij, 1999), and/or loss from roughened surfaces (White et al., 1996) followed by a typical slow release of these elements with bulk silicate weathering (Skorina and Allanore, 2015; Sparks, 1991). Warm-room leachate shows higher initial concentrations than cold-room leachate for K and Ca, which is likely the result of temperature and pH controls on desorption and mineral degradation (Brazier et al., 2019; Dreybrodt et al., 1996; Gaillardet et al., 2019; Lasaga, 1984; Li et al., 2021; White and Brantley, 1995).

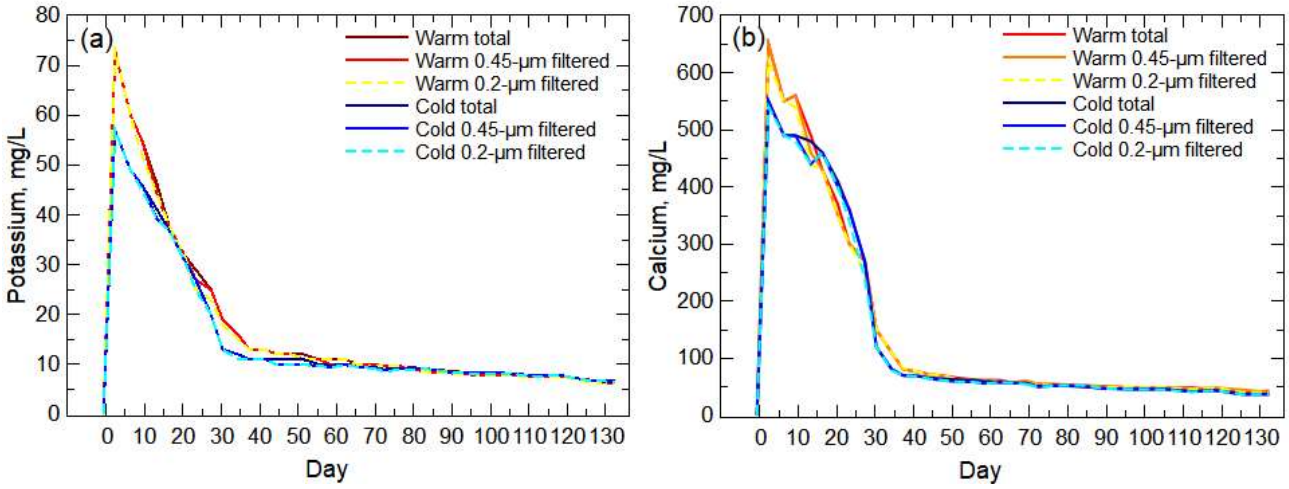

Figure 13. Potassium (a) and calcium (b) unfiltered (total) and filtered concentrations for the unamended, warm-room and cold-room leachate during the 20-week leach column experiment.

4.6 Complex Weathering

Iron concentrations for unamended, warm- and cold-room leachate indicated multiple weathering processes causing the release of Fe over the course of the experiment (Fig. 14). Iron content in the Wasatch and Fort Union waste rock is substantial (Fig. 7) and likely has multiple mineral sources, including sulfides (pyrite) and aluminosilicates (feldspars and associated clays) along with sorbed Fe (oxyhydr)oxides. The relation of Fe and Eh was moderate to weak, negative correlation (Spearman's ρ of −0.31 for the filtered concentrations and −0.11 for the unfiltered concentrations), likely as a result of the variety of Fe sources and solubility controls on Fe. Given the low solubility of Fe^{3+} in oxidizing and near-neutral pH (Hem and Cropper, 1962; Schwertmann, 1991), Fe likely was released from the waste rock as desorbed Fe (oxyhydr)oxides particles early in the experiment, which accounts for the large total Fe concentration peaks at Day 3. The potential for mobile Fe forms is a complex interaction of environmental conditions and solute composition and concentrations that commonly results in the formation of nanoscale to colloidal Fe particles (Davison, 1993; Gaffney et al., 2008; Hassellöv and von der Kammer, 2008; Liang and Morgan, 1990; Perret et al., 2000). The much larger concentration of Fe in the warm-room leachate during the initial peak contained substantially higher total Fe concentrations during this first week of the experiment indicative of the effect of pH and temperature on Fe-particle desorption and transport (Hatje et al., 2003; Possemiers et al., 2016; Weber et al., 2010). After the initial peak of Fe, there is a substantial release of Fe from the warm-room leachate with oxidation of the pyrite that is lessened under colder temperatures (Sun et al., 2015). As Fe forms are mobilized and removed from the waste rock along with reduction of available sulfide surfaces, Fe starts to weather at a consistent and lower release rate at approximately Day 65 (Fig. 14) similar to the trends of Ca and K during the later part of the experiment (Fig. 13a, b). This is potentially the result of residual microparticle flushing of pyrite, as seen in late-stage weathering of As until Day 98 (Fig. 11c) and the release of Fe (oxyhydr)oxide particles with weathering of the bulk solids and continued

desorption and particle aggregation/de-aggregation with transport (Journet et al., 2008; Wang et al., 2018).

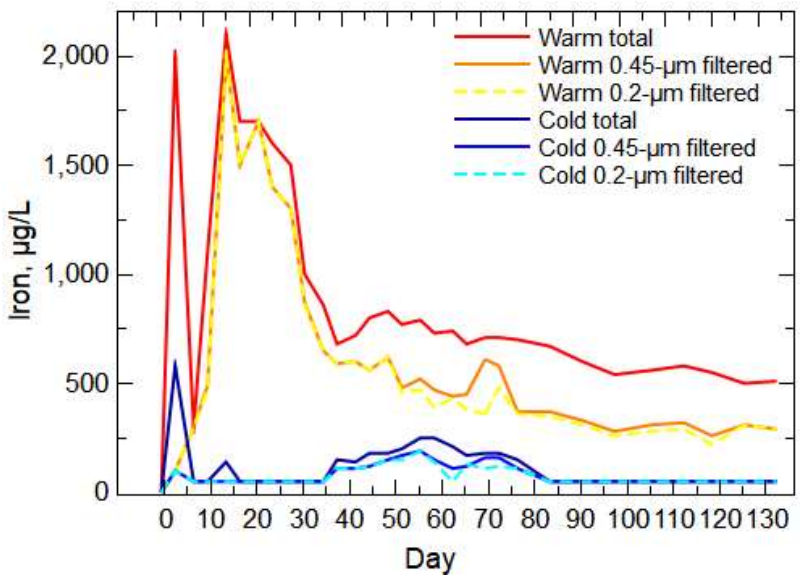

Figure 14. Iron unfiltered (total) and filtered concentrations for unamended, warm-room and cold-room leachate during the 20-week leach column experiment. Non-detect values were set to half the reporting limit (50 µg/L).

Chapter 5. Geochemical Modeling

5.1 Predictive Modeling

PHREEQC was used to evaluate sources of the contaminants As and Se that can be found in the Fort Union and Wasatch formations. The PHREEQC modeling program is based on the calculation of equilibrium between aqueous solutions and minerals, gases, solid solutions, exchangers, and sorption surfaces. Simplified forward (kinetic reaction) models were created for As and Se based on the perceived sources in the overburden formations and aligned with the mass of each element released from this study's unamended, warm-room leach column. Such models represent a likely predictive model for estimating potential impacts to water quality with weathering of the Wasatch and Fort Union waste rock given published information. Enhanced forward models were constructed to account for new mineral surfaces/nanomaterials given the substantial alteration of the overburden during mining. The goal was to compare typical weathering models built around As and Se release from known sources and enhanced weathering models focused on replicating the contribution from the weathering of new mineral surfaces and nanomaterials. For comparison to the benchtop leach column experiment, the initial As and Se mole values of the models were set to the accumulated release of the As and Se derived from the analyzed leachate of the unamended, warm-room leach column. The model evaluation consisted of comparing the temporal trends of modeled As and Se concentrations to the As and Se released from the leach column. The goal of the modeling was to identify the model parameters that would replicate new mineral surfaces/nanomaterials with weathering of the Wasatch and Fort Union waste rock. The model application used PHREEQC's capability to simulate the dynamic process of reaction kinetics (e.g., RATES and KINETICS code blocks) to reflect contributions of the contaminant sources within the waste rock.

5.2 Model Parameters

Four forward models were constructed with PHREEQC—As-bearing pyrite oxidation, As-bearing pyrite oxidation + nanomaterial contribution, Se-bearing gypsum dissolution, and Se-bearing gypsum dissolution + nanomaterial contribution. Each model combined a well-oxygenated, neutral water at 20 ºC with likely As and Se sources found in the Wasatch and Fort Union formations. The initial (basic) predictive models were built around geochemical reactions of bulk solid source of each of the contaminants—As-bearing pyrite (95% pyrite + 5% loellingite [$FeAs_2$]) and Se-bearing gypsum (95% gypsum + 5% nestolaite [$CaSeO_4$]). Arsenopyrite was not chosen for the oxidation reaction because it has not been identified in Powder River Basin coal and is structurally different (monoclinic and prismatic) compared to As-bearing pyrite (pyrite = cubic and diploidal + loellingite = orthorhombic and dipyramidal). The available amount of an As-bearing pyrite and Se-bearing gypsum were set to the total release of As or Se from the leach column to align output scales for comparison of the temporal trends. The initial As model was established as an oxidative dissolution of the As-bearing pyrite based on parameters described by Williamson and Rimstidt (1994). The initial Se model was established as the simplified dissolution of a dissolvable salt (log k = –7) given an initial area (A_0) to volume (V) ratio of 1.67 and an initial molar concentration (m_0). The log k value is smaller than the gypsum log k (–4.5) or hydrated nestolaite log k (–4.6) present in the LLNL database (PHREEQC available database), but such a value balances the reactivity of gypsum and nestolaite with availability of the mineral surface. This simplified reaction rate removes concerns regarding surface area availability and roughness while conveying the likelihood of the substantial dissolution of the gypsum following production of the

waste rock and reconstruction of the backfill aquifer that can produce very small and roughened particles from blasting, removal, and backfilling but still retain bound minerals that lessen overall source reactivity. The saturation index of gypsum was not incorporated into the reaction rate (negative feedback) given the limited amount of reacted gypsum (no saturation of the mineral given concentrations in the leachate from the column). These parameters and reaction rate were tested against the leach column results to evaluate the applicability of the model parameters for replicating the initial reaction and release of Se (dominant surface reaction as opposed to a surface-diffusion reaction (Lebedev, 2015)) that was expected during the early weathering stage of the leach column.

5.3 Initial Arsenic Modeling vs Leach Column Results

The initial As model did not produce an output trend similar to any of the As trends (unfiltered or filtered) in the column leachate (Fig. 15). The model produced an As trend that would be expected from unweathered, As-bearing pyrite with a relatively quick peak followed by a slow decline in concentration. The unfiltered and filtered As values in the leachate indicate an initial peak (or shoulder) followed by a larger peak before a substantial drop in As release near Day 20 (unfiltered) or Day 24 (filtered values). The unfiltered As trend is more variable compared to the filtered As trends likely because of particle transport moving through the leach column that contributes to the difference between the unfiltered and filtered concentrations throughout much of the experiment. The two-peak release (shoulder and main peak) of the As trend in the leachate likely occurs because of multiple source contributions, such as initial nanoparticle transport (no differences in unfiltered or filtered As concentrations during the first week) and the subsequent degradation of the sulfide mineral source with oxidative dissolution of As-bearing pyrite.

The delay in As release from degradation of As-bearing pyrite between the modeled oxidative dissolution process and the second peak of the leachate As trend likely is a result of the multi-step release of As from pyrite where As is initially released from the degrading mineral as a non-soluble species (As^{3+} or AsO_3^{-3}) that will be sorbed prior to full oxidation to the more soluble As^{5+} or AsO_4^{-3} (Cen et al., 2022; Silva et al., 2017). Arsenic released from the pyrite mineral structure can be retained by co-precipitation (e.g., ferric arsenates) and adsorption to Fe-(oxyhydr)oxides slowing As release into solution (Tabelin et al., 2020). Additionally, Cen et al. (2022) found that the release of As^{3+} from the oxidative dissolution of arsenopyrite is decreased by presence of biochar, a similar inorganic/organic carbon form to coal. Such factors indicate the likelihood of the limiting of As release until full oxidation of the element and degradation or transport of sorbing surfaces. Therefore, the two weathering processes for explaining the dual peak visible in the As released from the leach column likely is an initial transport of As as nanoparticles (e.g., sorbed to Fe (oxyhydr)oxides or As-bearing nanopyrite) followed by the greater release of As with the oxidative dissolution of the bulk As-bearing pyrite, and a subsequent slow decline as the sulfide mineral surface is decreased with further weathering.

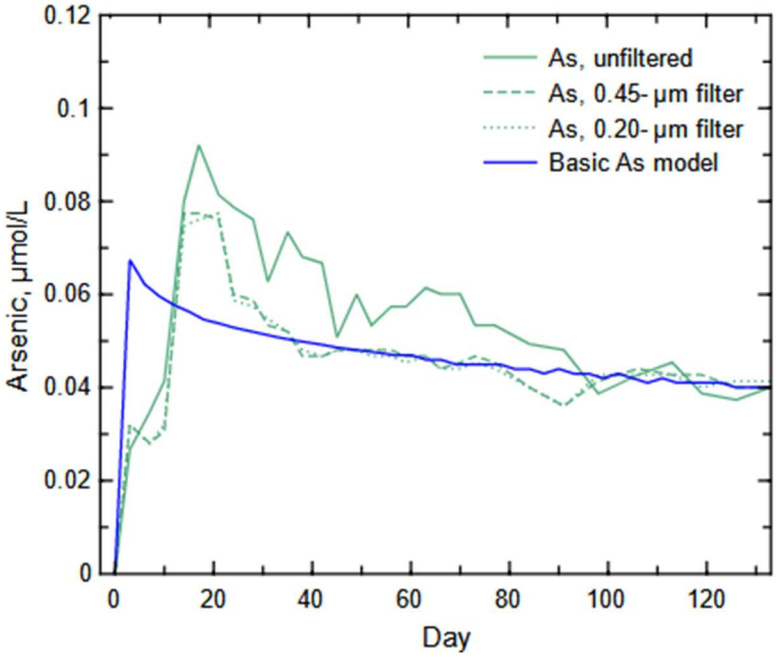

Figure 15. Arsenic results for basic arsenic model with oxidative dissolution of arsenic-bearing pyrite and total (unfiltered) and filtered arsenic concentrations in the leachate from the unamended, warm-room leach column.

5.4 Enhanced Arsenic Modeling vs Leach Column Results

The weathering regime to be tested with the enhanced model reflects a difference in availability of bulk solid and particle As to capture the two peak trend identified in the leachate results (Fig. 15). An examination of the release of total Fe from the waste rock indicates a similar trend with two peaks during the first 30 days of the experiment (Fig. 16). There appears to be a flushing of microparticles of Fe, and likely As, although the Fe 0.45-µm concentrations were also substantial during the first peak compared to the mass of As. The initial peak of As and Fe likely is the result of the flushing of micro- and nano-particles from the system prior to the onset of oxidative dissolution of the As-bearing pyrite and release of As into solution. This flushing of As and Fe is a result of the association of As and Fe where As is commonly sorbed to Fe, in particular Fe (oxyhydr)oxides (Bisone et al., 2016). Nanomaterial Fe (oxyhydr)oxides are common and have a high surface energy that will readily sorb other metal(loid)s, such as As (Hochella Jr. et al., 2019; Navrotsky et al., 2008; Waychunas et al., 2005).

The enhanced model (Figure 17) for As release incorporated the particle contribution through dissolution of a soluble salt to replicate nanoparticle desorption (initial concentration peak) and As release from the oxidative dissolution of pyrite (second concentration peak). The modeled As release trend is similar to the filtered As release trend in the leachate, although a larger release of As is present in the leachate during the second peak. This additional mass of As in the filtered leachate likely is the continued release of As-bearing particles that move through the low permeability waste rock (2-hr drain period was necessary to capture drainable water from the approximate 0.5-m column of saturated waste rock). The removal of transportable particles from the column and reduction of the early availability of a substantial portion of pyrite surface area produced a post-Day 30 weathering trend representative of the slow release of As from pyrite oxidation as available surface area is reduced.

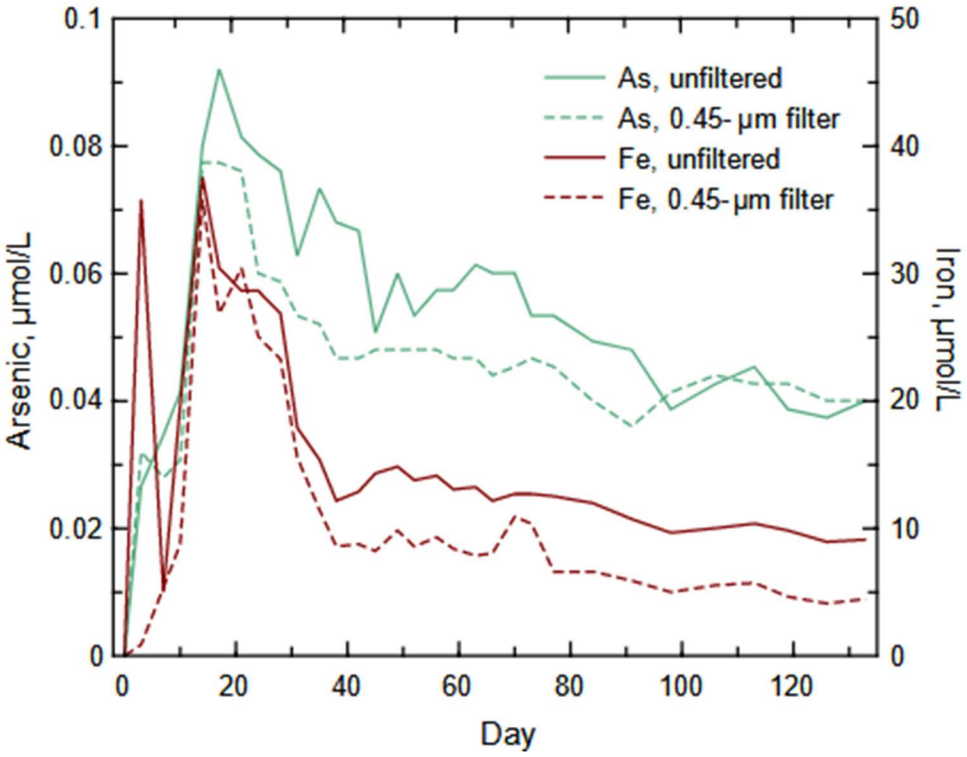

Figure 16. Iron and arsenic concentrations in unfiltered and 0.45-µm filtered leachate collected from the unamended, warm-room leach column.

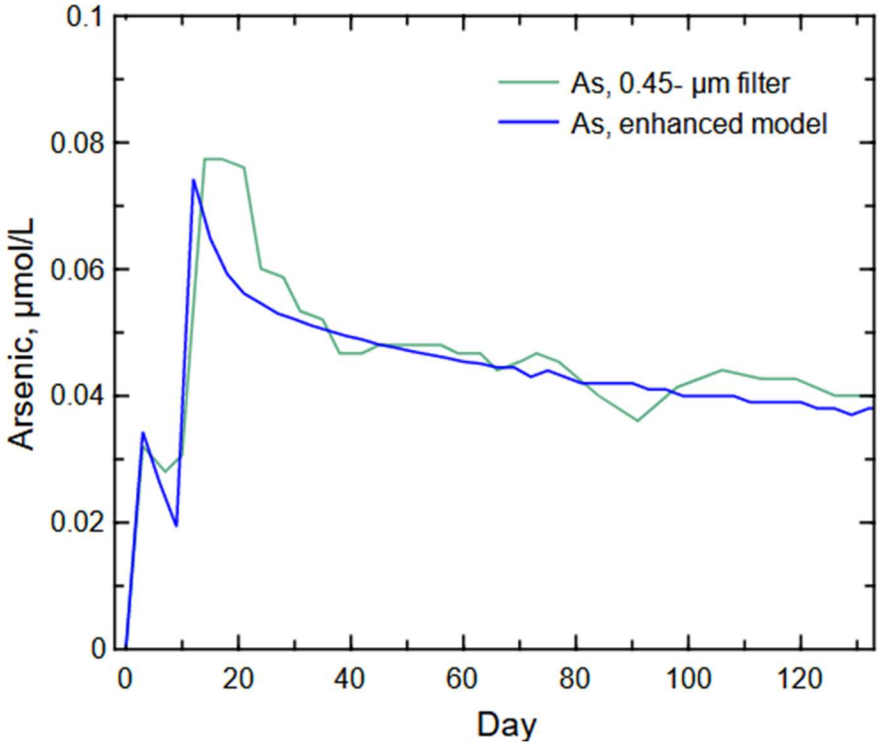

Figure 17. Arsenic concentrations predicted from the enhanced arsenic model of desorption/salt dissolution and oxidative dissolution of arsenic-bearing pyrite compared to the filtered (< 0.45 µm) arsenic concentration released from the unamended, warm-room leach column.

5.5 Initial Selenium Modeling vs Leach Columns

The leach column produced similar Se concentrations for the total, 0.45-µm filtered, and 0.20-µm filtered concentrations. The presence of Se salts in the waste rock (Dreher and Finkelman, 1992b; Y. E. Yudovich and Ketris, 2006) and the results of the leach column suggest that Se was present in the leachate as Se ions or < 200 nm nanoparticles. The Se results for the leach column produced an initial spike in Se concentrations that quickly declined to very low concentrations by Day 10 and non-detectable levels by Day 21 (Fig. 18). Such a quick Se release and decline are indicative of a fast mineral reaction and release of the solute (e.g., salt dissolution) or flushing of a nanomaterial source. The oxidative dissolution of a Se-containing sulfide would not be expected to produce such quick release because such a source would produce a temporal trend similar to the slower increase and decrease model output shown in Figure 15 (As-bearing pyrite oxidative dissolution). Given the solubility of selenate, limited mobility of selenite, and oxygenated conditions recorded during the period when Se was present in the leachate (first 17 days), it is expected that Se in the leachate was primarily present as selenate derived from dissolution of Se salts.

The initial Se model was based on dissolution of a Se salt (95 % gypsum + 5 % nestolaite [$CaSeO_4$]) given the presence of substantial gypsum in the waste rock formations and noticeably quick release of Se with weathering of the waste rock in the leach column experiment. The basic model of Se salt dissolution produced a similarly quick concentration peak present in the leachate, but the modeled Se release trend indicated that all Se was quickly released in one peak concentration, not the quick concentration peak and slower concentration decline visible in the leachate Se trend (Figure 18). This contrast in Se release trend is suggestive a second, yet slightly slower process of Se release from the waste rock in addition to the Se salt dissolution.

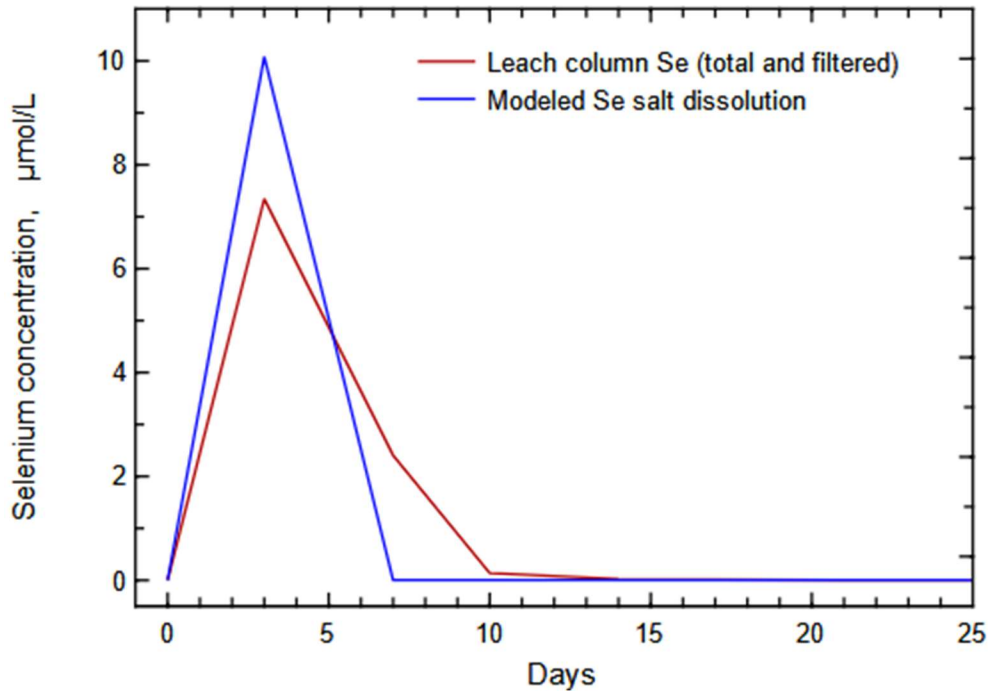

Figure 18. Comparison of the modeling of a selenium salt dissolution and results from the unamended, warm-room leach column. Concentrations recorded from the leach column were the same for the total, 0.45-µm filtered, and 0.2-µm filtered concentrations.

5.6 Enhanced Selenium Modeling vs Leach Columns

The initial model was capable of identifying the timing of the Se peak in leach column results but not a post-peak decline of concentrations (Fig. 18). A model of salt dissolution and bulk solid Se-containing pyrite would not replicate the leach column results but simply add to the peak concentration followed by smaller concentrations over a longer period of time similar to the As release from oxidation of bulk solid pyrite. An enhanced model of Se salt dissolution (part of peak concentration) and oxidation of Se-containing nanoparticle pyrite (area-to-volume (A/V) ratio of 4.2) was able to replicate the leach column results (Fig. 19). The enhanced model clearly identified a peak concentration from salt dissolution and enhanced release of Se with nano-pyrite oxidation with near replication of the post-peak decline (Fig. 19). An increase of the A/V ratio from the standard 0.3 value used for the geochemical databases (Williamson and Rimstidt, 1994) represents a substantial increase in potential weathering with generation of nanomaterials in backfill waste rock. Nanomaterials can be highly reactive because as size decreases, the A/V ratio substantially increases allowing for a much greater available surface for reactions (Plathe et al., 2013). The change in particle size during alteration from waste rock generation should depend on the mineral type, composition, and original particle shape (Hochella Jr et al., 2008).

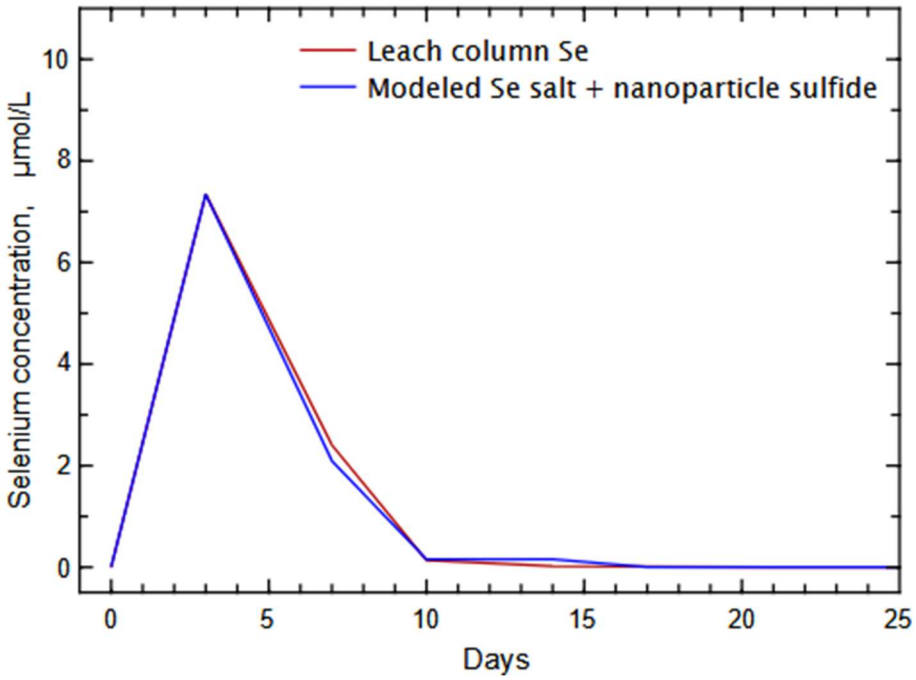

Figure 19. Comparison of the modeling of a selenium salt dissolution + nanomaterial contribution and results from the unamended, warm-room leach column.

Chapter 6. Amendments

Given laboratory and modeling results that indicate the generation of new mineral and nanomaterial sources of potential contaminates for backfill aquifers constructed from Powder River Basin waste rock, available amendments to the waste rock were tested in the laboratory under the warm-room column conditions. The amendments—soil, zeolite, compaction, rinse—were considered as possible treatments to the waste rock prior to or during construction of the backfill aquifers. A soil layer is present in the overburden that could be separated during overburden removal and added as a layer-specific amendment during backfill. Similarly, zeolite is a readily available soil amendment that has a long history of being used to reduce the transport of cationic metal(loid)s (Chmielewská, 2019; Jiang et al., 2018; Margeta et al., 2013; Wang and Peng, 2010) and could be added as a layer-specific amendment during backfill. Compaction was tested as a possible amendment with the consideration of enhanced construction techniques to increase compaction during backfill and landscape reconstruction to lessen available groundwater pathways that could interact with the newly available mineral surfaces and nanomaterials. The last amendment, rinsing, is a difficult treatment for construction of backfill aquifers, but was considered as a possible treatment if backfill construction is delayed, exposing the waste rock to longer surface weathering where runoff could be captured and treated given the likelihood of mobilized contaminants from the new mineral and nanomaterial sources.

The Eh trends for all amended and unamended, warm-room leach columns were similar throughout the experiment (Fig. 20). The zeolite-amended column released leachate with the highest pH and alkalinity throughout the experiment likely because of the release of hydroxyl groups (S-OH) associated with the $(Si,Al)O_4$ tetrahedra of the zeolite as solutes undergo sorption/desorption (Szekeres and Tombácz, 2012). In contrast to other columns, soil-amended leachate displayed a period of relatively high specific conductance from Day 23 until Day 90 (Fig. 20b), indicating a potentially longer flushing of dissolved ions or nanoparticles that likely originated from the soil.

Leachate from the soil-amended column had the highest peak concentrations of chloride, fluoride, and nitrate (Fig. 21a, b, and c). Leachate from the compacted column and the rinsed column had similar peak concentrations of chloride and sulfate (Figure 21a and d) that were lower than concentrations in leachate from the remaining columns. All amended-column leachate contained higher peak concentrations of fluoride compared to the unamended-column leachate (Figure 21b). Leachate from the soil- and zeolite-amended columns contained the largest peak chloride concentrations—29 mg/L and 25 mg/L, respectively—compared to the unamended column peak concentrations of 22 mg/L. Leachate from the compacted and rinsed columns had the lowest peak concentrations of chloride at 16 mg/L and 17 mg/L, respectively. Peak nitrate concentrations in leachate from the unamended-, zeolite-, and compacted-column were similar at approximately 17 mg/L with the rinsed-column leachate containing a peak concentration of 12 mg/L and the soil-amended leachate had a peak concentration of 37 mg/L (Fig. 21c). All column leachate indicated sulfate peak concentrations > 44,000 mg/L except for leachate from the zeolite-amended column where sulfate concentrated peaked at 3,900 mg/L. Sulfate results support the assumption of substantial gypsum present in the waste rock discussed as a potential source of Se (Section 4.3).

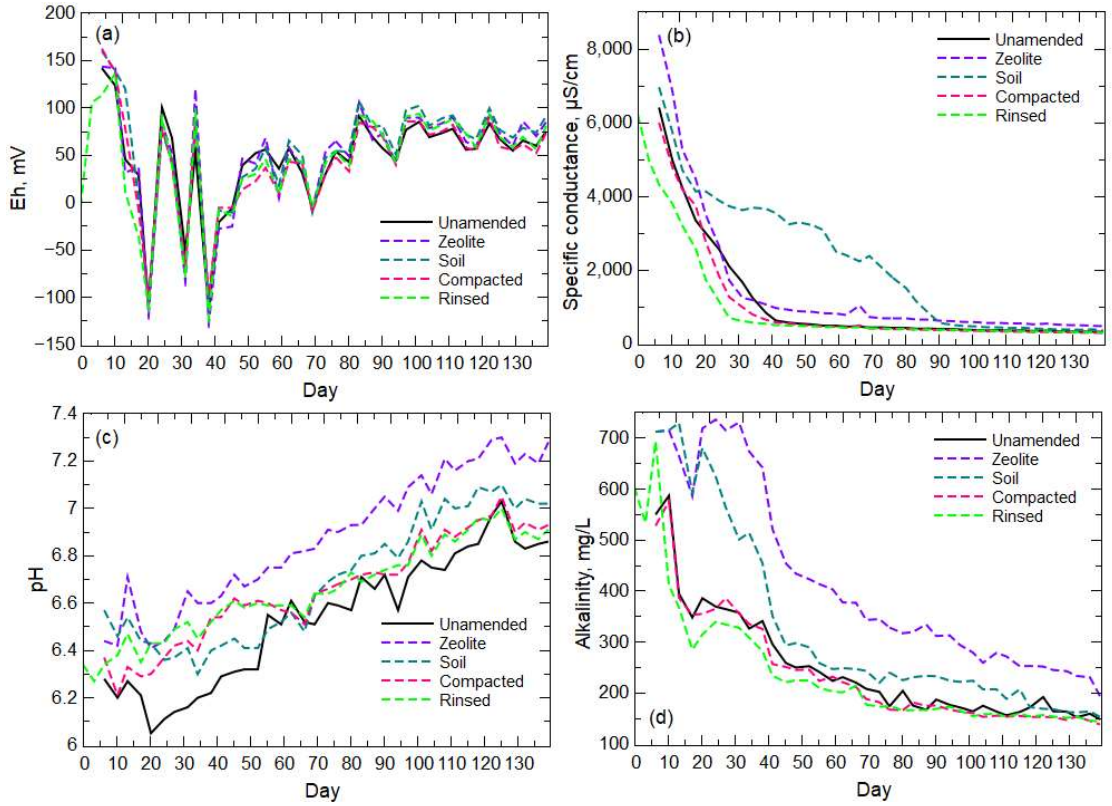

Figure 20. The field parameter results for (a) Eh, (b) specific conductance, (c) pH, and (d) alkalinity of leachate for unamended and amended columns.

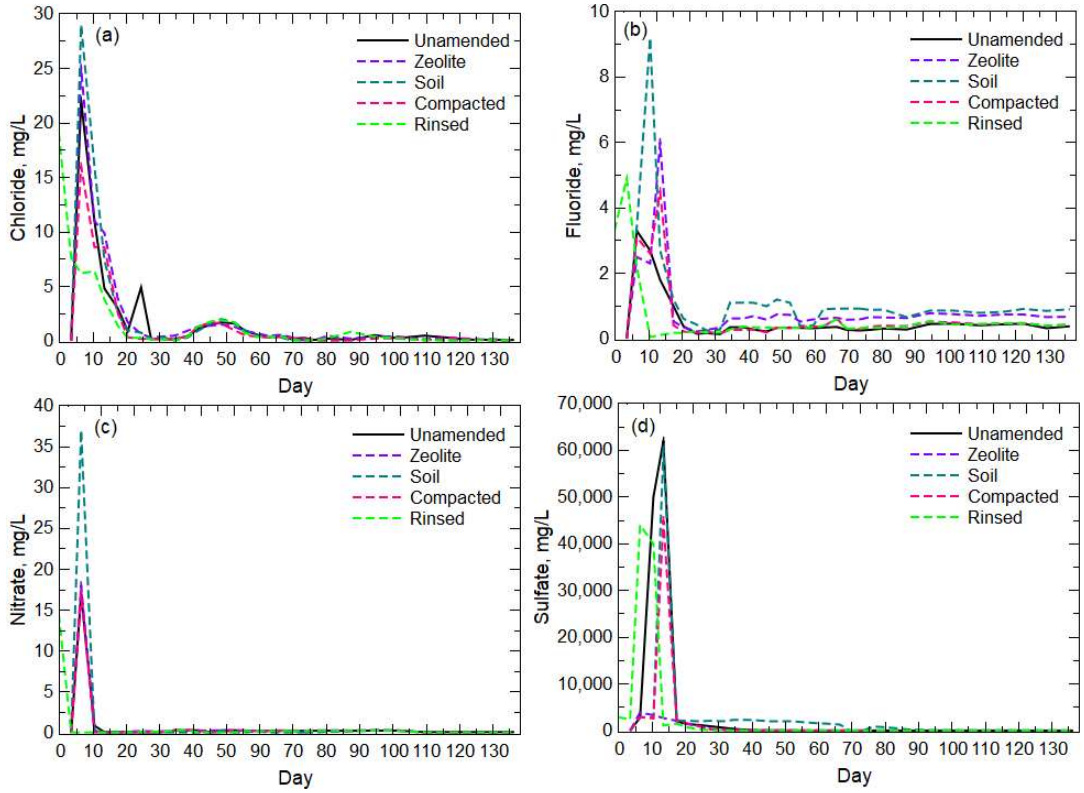

Figure 21. Anion concentration results for unamended and amended columns for (a) chloride, (b) fluoride, (c) nitrate, and (d) sulfate.

Metal(loid) concentrations in the leachate from the amended columns varied according to the source (e.g., pyrite oxidation vs nanoparticle release) and amendment that produced different influences depending on the metal(loid) solute. Arsenic concentrations for leachate from the zeolite-amended column (Fig. 22a) indicated consistently larger values of As compared to leachate from the other amendments and the leachate from the unamended column (Figure 11). The double peak trend of As release noted in Chapter 5 was present in the leachate from the amended columns for all unfiltered and filtered concentration trends except for the rinsed amendment. The leachate from the soil-amended column (Fig. 22b) indicated a greater divergence between unfiltered and filtered concentrations, indicating a likely substantive particle source that was released from the column with continued flushing. Both compacted and rinsed columns (Fig. 23c, d) had arsenic concentrations in the leachate with lower concentrations than the unamended leachate, as well as reduced peaks and relatively consistent post-peak concentrations compared to the unamended column leachate (Figure 11).

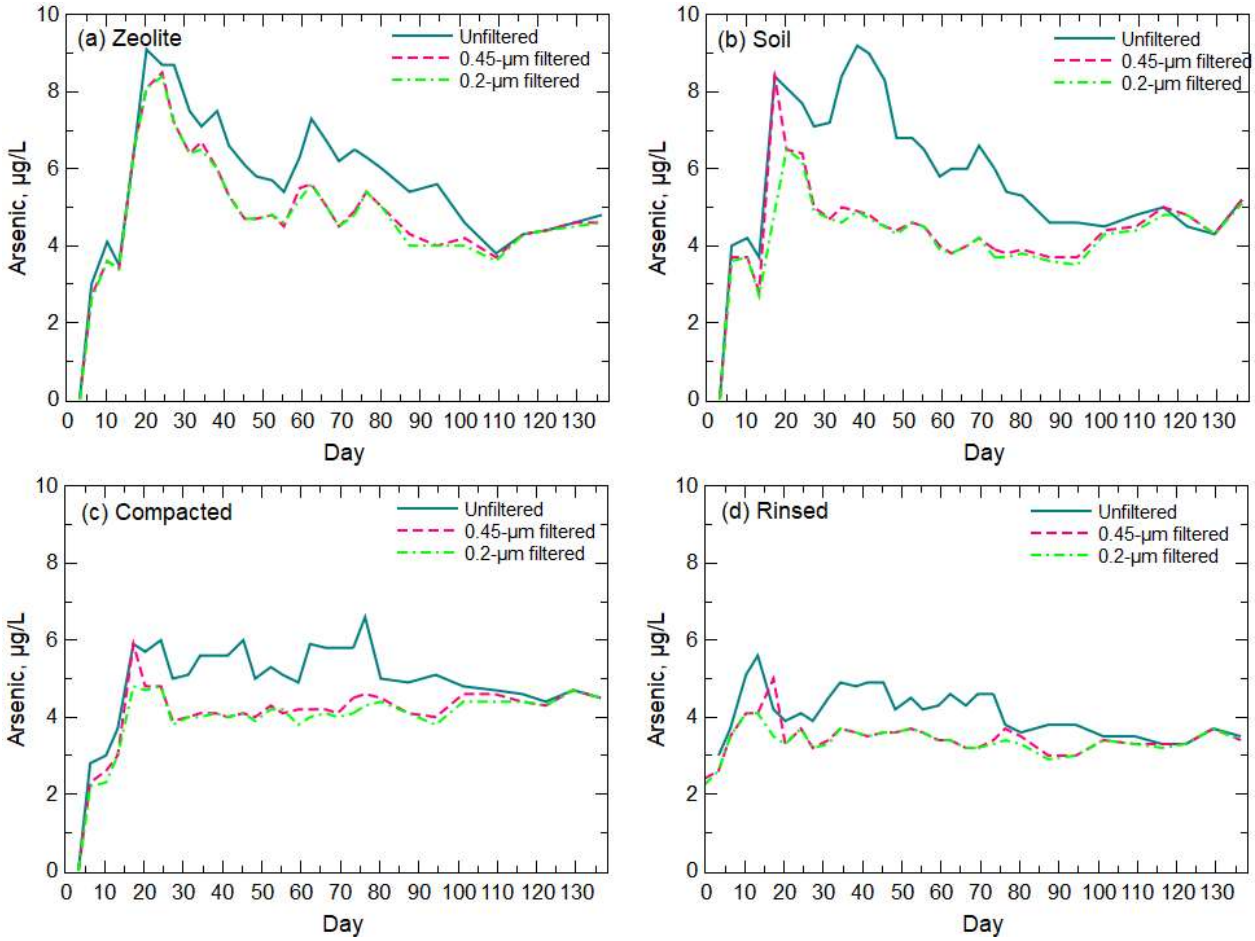

Figure 22. Arsenic concentrations for (a) zeolite, (b) soil, (c) compaction, and (d) rinsed amended columns. Non-detection values were set to half the reporting limit (0.5 µg/L).

Cadmium concentrations in leachate from amended columns (Figure 23) indicated a similar trend as the unamended leachate (Figure 11), which consisted of an initial peak followed by a quick decline below reporting limits. However, zeolite and soil amendments produced lower concentrations than the unamended column leachate, and zeolite and compacted column leachate indicated no difference between unfiltered and filtered concentrations. Compacted and rinsed

column leachate contained a similar peak value with the unamended column value of 1.4 µg/L, and the rinsed column leachate indicated a similar divergence of unfiltered and filtered concentrations as the unamended leachate (Fig. 11).

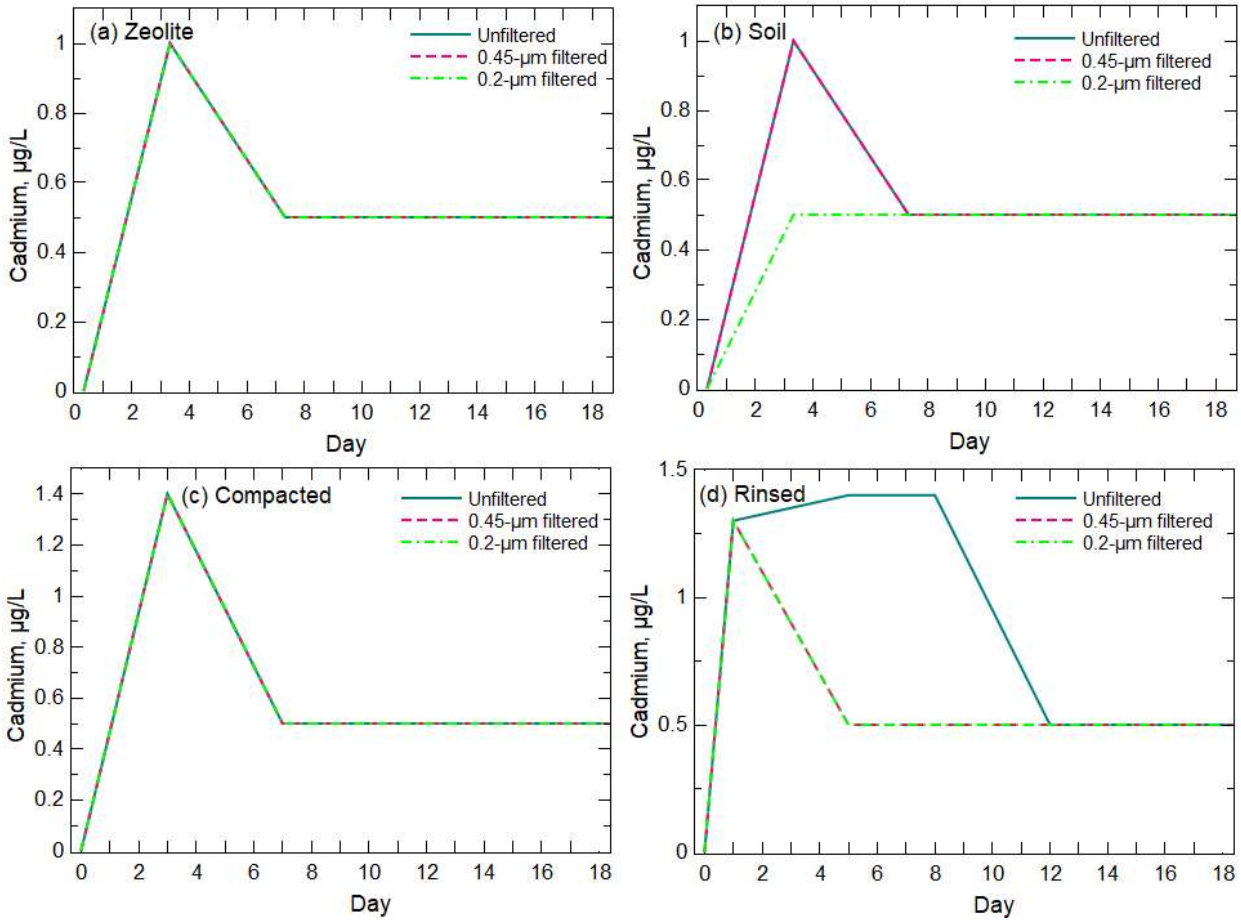

Figure 23. Cadmium concentrations in leachate from (a) zeolite, (b) soil, (c) compaction, and (d) rinsed amended columns for the first 18 days of the experiment. Non-detection values were set to half the reporting limit (0.5 µg/L).

For Fe concentrations, the zeolite amended leachate (Fig. 24a) filtered concentrations (0.45-µm and 0.2-µm filtered) fall below reporting values by Day 32 while its total (unfiltered) concentrations stay relatively high, not following the unamended column leachate trend that displays equilibration as it nears the end of the experiment. The soil amended column (Fig. 23b) shows a slower increase and decrease compared to the other amended and unamended columns, displaying a lower concentration peak. The compacted column (Fig. 24c) illustrates the highest concentration, 2,200 µg/L of both amended and unamended column leachate on Day 14 but seems closest in trend to the unamended column leachate. Rinsed column leachate (Fig. 24d) also shows a similar trend to the unamended column but equilibrates at a lower concentration with more filtered value variation. None of the amended columns illustrate an initial double peak compared to the unamended column, but unfiltered concentrations diverge from filtered concentrations at various times and magnitudes for Fe in all amended and unamended columns.

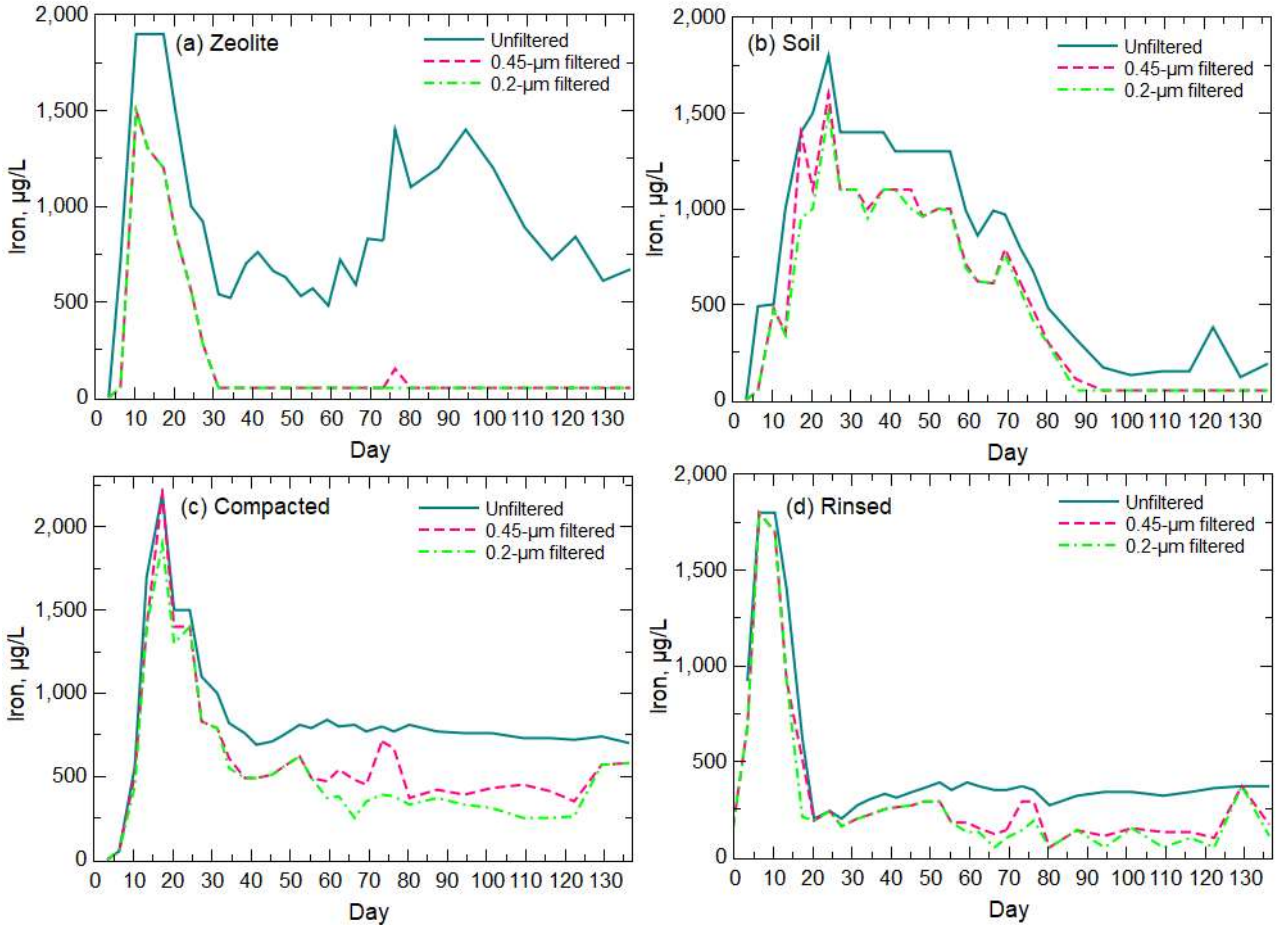

Figure 22. Iron concentrations for (a) zeolite, (b) soil, (c) compaction, and (d) rinsed amended columns. Non-detection values were set to half the reporting limit (5 µg/L).

Sodium concentrations for both amended and unamended column leachate show an initial peak followed by a fairly rapid decrease that varies in length by column, with little difference between unfiltered and filtered concentrations. The zeolite and soil amended (Fig. 25a, b) leachate displayed higher initial concentrations, 1,400 mg/L and 710 mg/L respectfully, of Na than the unamended leachate that peaks at 690 mg/L (Fig. 25e). The zeolite amended leachate also shows the highest concentrations consistently, never falling below reporting limits as it reaches equilibrium at a lower concentration of solute output. The lowest concentrations of Na are illustrated by the compacted column leachate, reporting its peak concentration at 590 mg/L.

Zinc concentrations of the unamended column leachate were surpassed by the initial peak of the soil-amended leachate (160 µg/L) and delayed peak (290 µg/L) of the zeolite amended leachate at approximately Day 74 (Fig. 26a). The compacted column leachate has the most similar peak and decline trend to the unamended column leachate, while the zeolite leachate differs the most from the unamended column in trend with a delayed peak.

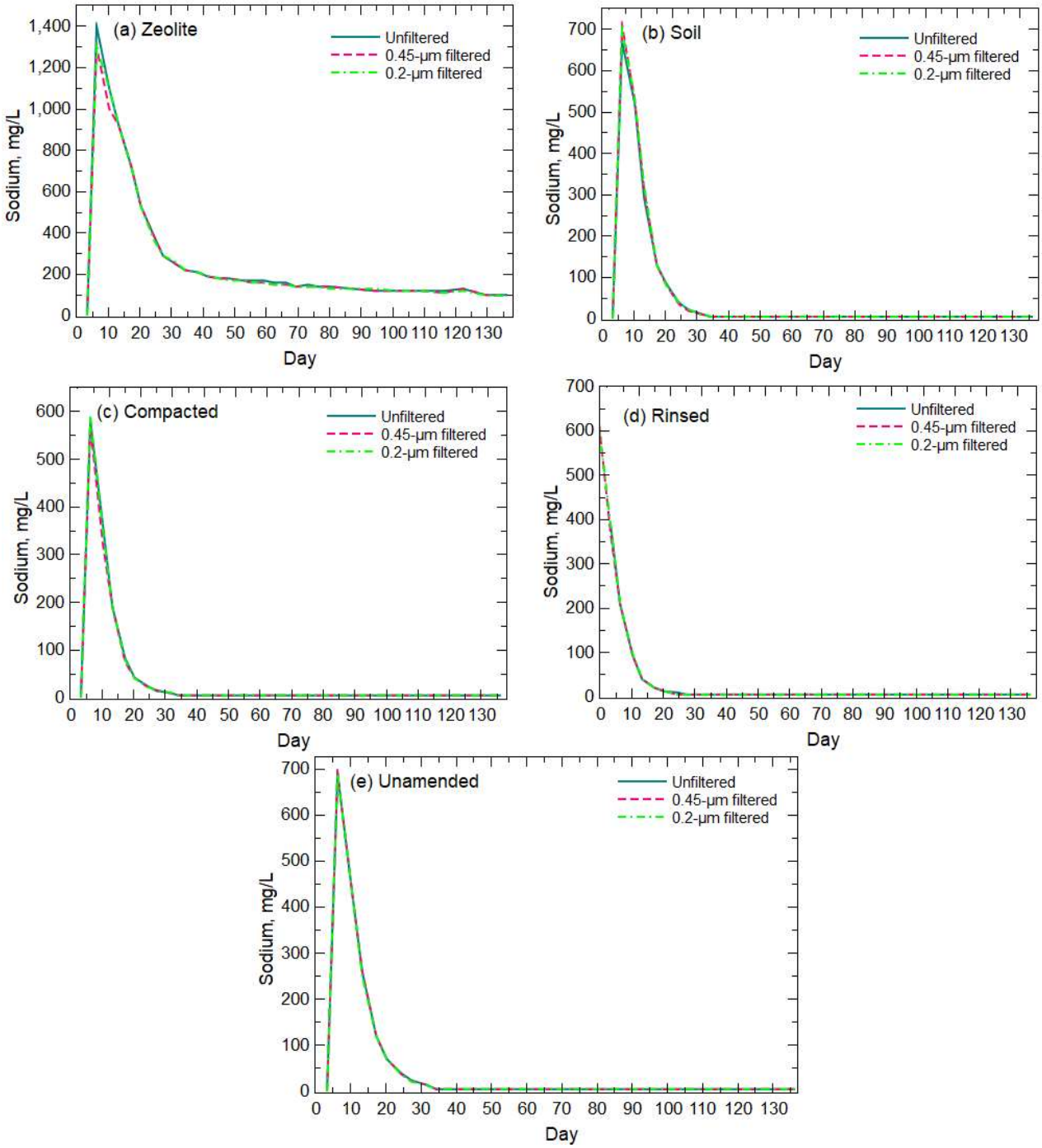

Figure 23. Sodium concentrations for (a) zeolite, (b) soil, (c) compaction, (d) rinsed, and (e) unamended columns. Non-detection values were set to half the reporting limit (5 mg/L).

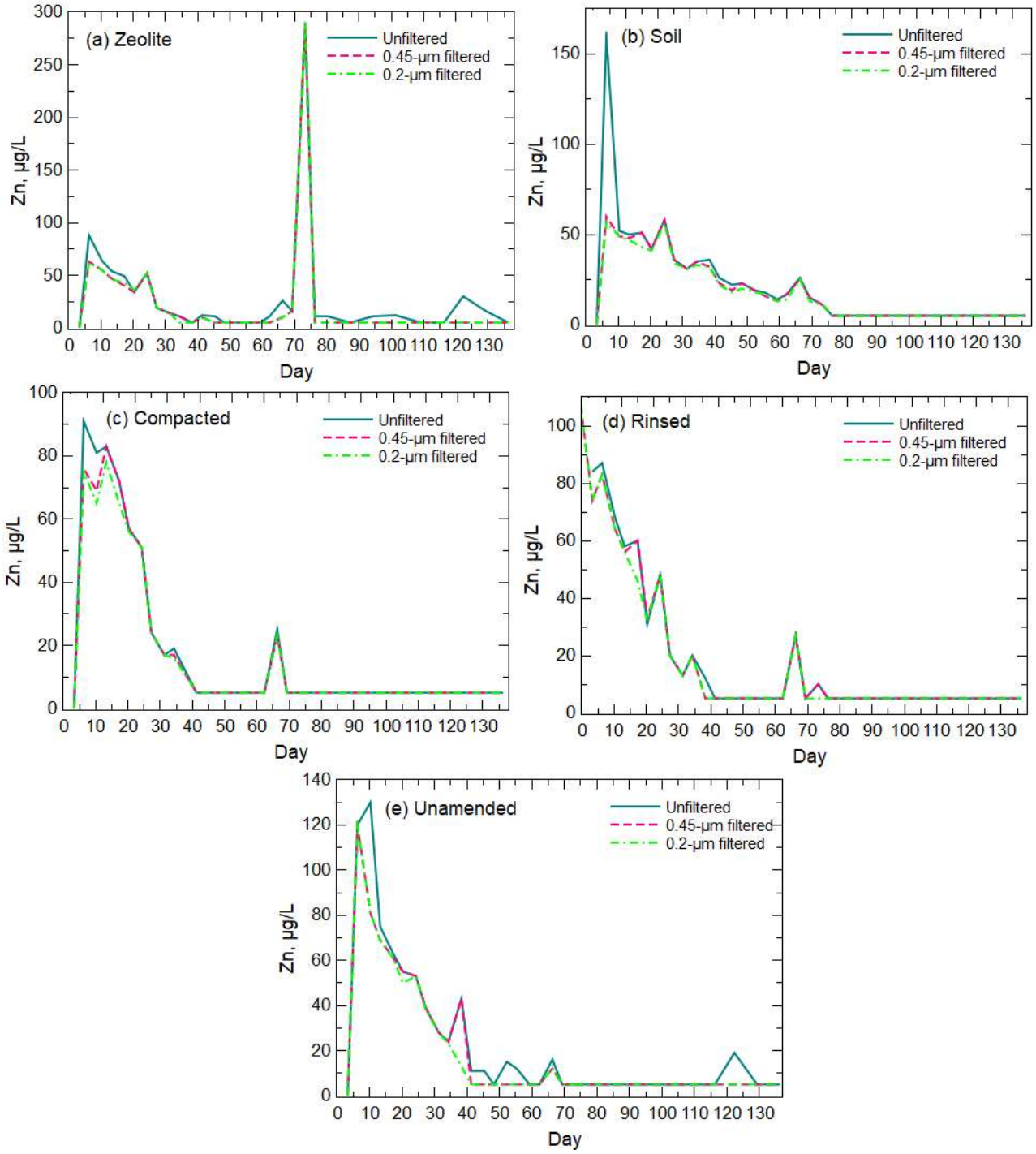

Figure 24. Zinc concentrations for (a) zeolite, (b) soil, (c) compaction, (d) rinsed, and (e) unamended columns. Non-detection values were set to half the reporting limit (5 µg/L).

Chapter 7. Conclusions

Restoration of open-pit mines may utilize waste rock for landscape reconstruction, which can include the construction of backfill aquifers. Weathering and contaminant transport may be different in backfill aquifers compared to the surrounding aquifer because of newly available mineral surfaces and transportable nano- to micro-scale particles generated during mining. Waste rock from the Cordero Rojo open-pit coal mine in the Powder River Basin was exposed to benchtop leachate experiments for 20 weeks at temperatures of 5 °C and 20 °C. Collected leachate was analyzed for Eh, pH, specific conductance, alkalinity, and cation and anion concentrations as unfiltered and 0.45-µm and 0.2-µm filtered concentrations. During the experiment, leachate Eh and pH substantially varied during the first 55 days, which corresponds to a period of high specific conductance (> 1000 µS/cm) and alkalinity (> 200 mg/L). Correspondingly, anion and cation concentrations were the largest during this early weathering stage, and the filter fractions indicated multiple forms of transported elements. After this early weathering stage, all environmental parameters evolved towards a weathering equilibrium of neutral, oxidizing, and low solute conditions indicated by positive Eh values, pH near 7, and specific conductance < 500 µS/cm. This evolution was reflected in the decline and stabilization or non-detection of metal(loid) concentrations reflective of a shift to primarily bulk aluminosilicate weathering when coal- and salt-associated elements, such as arsenic, cadmium, and selenium, were not detected or at minimal concentrations. Over the course of the experiment, the solute trend of certain elements indicated particular weathering processes—cadmium and nanoparticle transport, selenium and salt dissolution, and arsenic and pyrite oxidation. The mining of the overburden formations can create newly available mineral surfaces and nanomaterials that will weather to produce solutes not typically found in the regional groundwater contained in these formations.

The complexity of predicting the water quality of a backfill aquifer following landscape reconstruction is a result of the alteration of the waste rock from its overburden geologic state to its post-mining deconstructed state. The alteration of the material exposes previously bound mineral surfaces that may have high reactivity and produces nanomaterials that can be transported and have high reactivity because of the large surface-to-volume ratio. These newly available sources of the contaminants may result in substantial releases of the contaminants early in the weathering of the backfill aquifer. Traditional geochemical modeling of known contaminant sources in the overburden can capture the primary process of mineral weathering and contaminant release, but the identification and inclusion of nanomaterial contributions to contaminant release are necessary to evaluate the potential for water quality impacts. Enhanced geochemical models were constructed with likely nanomaterial sources to improve the potential prediction of select contaminants that were identified in the weathering experiments. The enhanced geochemical models were better able to replicate the release of the contaminants from the waste rock compared to a traditional geochemical model. For instance, an enhanced model for evaluating the potential release of arsenic incorporated the nanomaterial contribution through dissolution of a soluble salt to replicate nanoparticle desorption (new arsenic source) and arsenic release from the oxidative dissolution of pyrite (traditional or expected source). Additionally, an enhanced geochemical model was constructed to examine the release of selenium from the waste rock. This enhanced model paired the release of selenium from salt dissolution (new selenium source) and oxidation of nanoparticle Se-containing pyrite (traditional or expected source). The enhanced model clearly identified a peak concentration from salt dissolution and enhanced release of Se with oxidation of

a nanoparticle pyrite with near replication of the post-peak decline compared to the release trend of selenium from the weathering experiment.

The weathering experiment and the modeling of arsenic and selenium release from the Powder River Basin waste rock indicated a need to consider the possible release of contaminants into groundwater in backfill aquifers with the reconstruction of mine sites in the basin. Water chemistry likely will be different in the backfill aquifers compared to regional aquifers contained in the overburden material that is mined and used for landscape reconstruction. Four different waste rock amendments were evaluated for their potential influence on reducing solute release through similar leach column experiments as were conducted with the unamended waste rock. These amendments consisted of soil, zeolite, compaction, and rinsing. A soil layer is present in the overburden that could be separated during overburden removal and added as a layer-specific amendment during backfill. Similarly, zeolite is a readily available soil amendment that has a long history of being used to reduce the transport of cationic metal(loid)s and could be added as a layer-specific amendment during backfill. Compaction was tested as a possible amendment with the consideration of enhanced construction techniques to increase compaction during backfill and landscape reconstruction to lessen available groundwater pathways that could interact with the newly available mineral surfaces and nanomaterials. The last amendment, rinsing, is a difficult treatment for construction of backfill aquifers but was considered as a possible treatment if backfill construction is delayed, exposing the waste rock to longer surface weathering where runoff could be captured and treated. The leachate from the amended columns indicated that compacted and rinsed amendments were able to substantially reduce the release of solutes in comparison to the unamended leachate and the soil and zeolite amendments. The compaction amendment appears to restrict the flow of water, thereby restricting the interaction of water with the new contaminant sources in the waste rock. The compaction results indicate that landscape reconstruction would require greater heavy equipment use to further compact the backfill and provide a similar effect where the tested waste rock was subjected to a 10 % volume reduction compared to the unamended leach column (same mass of waste rock). The rinse amendment provides for flushing prior to weathering of the waste rock and would require a change in storage of the waste rock prior to landscape reconstruction, including collection of runoff from surface storage of waste rock. The length of additional surface exposure to precipitation and flushing of readily available solutes is unknown, but the rinsed amendment constituted two cycles of a 3-day saturation followed by full release of the rinse/leachate prior to start of the 20-week experiment. Soil and zeolite amendments did reduce the concentrations of select solutes compared to the unamended leach column, but these amendments did not consistently reduce the solute load of the leachate, particularly during the early weathering stage.

References

Acero, P., Ayora, C., Carrera, J., Saaltink, M.W., Olivella, S., 2009. Multiphase flow and reactive transport model in vadose tailings. Appl. Geochem. 24, 1238–1250. https://doi.org/10.1016/j.apgeochem.2009.03.008

Acero, P., Cama, J., Ayora, C., 2007. Sphalerite dissolution kinetics in acidic environment. Appl. Geochem. 22, 1872–1883. https://doi.org/10.1016/j.apgeochem.2007.03.051

Adams, M.B., Archer, V.A., Bailey, S., McGuire, K., Miniat, C.F., Neary, D.G., O'Geen, T., Robichaud, P.R., Strobel, M., 2020. Soils and Water, in: Pouyat, R.V., Page-Dumroese, D.S., Patel-Weynand, T., Geiser, L.H. (Eds.), Forest and Rangeland Soils of the United States Under Changing Conditions: A Comprehensive Science Synthesis. Springer International Publishing, Cham, pp. 33–49. https://doi.org/10.1007/978-3-030-45216-2_3

Agbenin, J.O., van Raij, B., 1999. Rate processes of calcium, magnesium and potassium desorption from variable-charge soils by mixed ion-exchange resins. Geoderma 93, 141–157. https://doi.org/10.1016/S0016-7061(99)00049-X

American Society for Testing and Materials, 2018a. Standard Practice for Reducing Samples of Aggregate to Testing Size. https://doi.org/10.1520/C0702_C0702M-18

American Society for Testing and Materials, 2018b. Standard Test Method for Laboratory Weathering of Solid Materials Using a Humidity Cell. https://doi.org/10.1520/D5744-18

American Society for Testing and Materials, 2016. Practice for Probability Sampling of Materials.

American Society for Testing and Materials., 2004. Test Method for Slake Durability of Shales and Similar Weak Rocks (No. ASTM D4644). ASTM International.

Anderson, S.P., Anderson, R.S., Hinckley, E.-L.S., Kelly, P., Blum, A., 2011. Exploring weathering and regolith transport controls on Critical Zone development with models and natural experiments. Appl. Geochem., Ninth International Symposium on the Geochemistry of the Earth's Surface (GES-9) 26, S3–S5. https://doi.org/10.1016/j.apgeochem.2011.03.014

Ayers, J., 1986. Lacustrine and fluvial-deltaic depositional systems, Fort Union Formation (Paleocene), Powder River basin, Wyoming and Montana. Am. Assoc. Pet. Geol. Bull. 70, 1651–1673. https://doi.org/10.1306/94886C90-1704-11D7-8645000102C1865D

Baerlocher, C., McCusker, L.B., Olson, D.H., 2007. Atlas of zeolite framework types, 6th rev. ed. Elsevier, Amsterdam.

Banwart, S.A., Evans, K.A., Croxford, S., 2002. Predicting mineral weathering rates at field scale for mine water risk assessment. Geol. Soc. Lond. Spec. Publ. 198, 137–157. https://doi.org/10.1144/GSL.SP.2002.198.01.10

Bao, Z., Al, T., Bain, J., Shrimpton, H.K., Finfrock, Y.Z., Ptacek, C.J., Blowes, D.W., 2022. Sphalerite weathering and controls on Zn and Cd migration in mine waste rock: An integrated study from the molecular scale to the field scale. Geochim. Cosmochim. Acta 318, 1–18. https://doi.org/10.1016/j.gca.2021.11.007

Bartos, T., Ogle, K.M., 2002. Water Quality and Environmental Isotopic Analyses of Ground-Water Samples Collected from the Wasatch and Fort Union Formations in Areas of Coalbed Methane Development—Implications to Recharge and Ground-Water Flow, Eastern Powder River Basin, Wyoming (Water Resources Investigations Report No. 02–4045). U.S. Geological Survey, Cheyenne, Wyoming.

Bisone, S., Chatain, V., Blanc, D., Gautier, M., Bayard, R., Sanchez, F., Gourdon, R., 2016. Geochemical characterization and modeling of arsenic behavior in a highly contaminated mining soil. Environ. Earth Sci. 75, 306. https://doi.org/10.1007/s12665-015-5203-z

Blowes, D.W., Jambor, J.L., 1990. The pore-water geochemistry and the mineralogy of the vadose zone of sulfide tailings, Waite Amulet, Quebec, Canada. Appl. Geochem. 5, 327–346. https://doi.org/10.1016/0883-2927(90)90008-S

Brazier, J.-M., Schmitt, A.-D., Gangloff, S., Pelt, E., Chabaux, F., Tertre, E., 2019. Calcium isotopic fractionation during adsorption onto and desorption from soil phyllosilicates (kaolinite, montmorillonite and muscovite). Geochim. Cosmochim. Acta 250, 324–347. https://doi.org/10.1016/j.gca.2019.02.017

Brownfield, M., Cathcart, J.D., Affolter, R.H., Brownfield, I.K., Rice, C.A., O'Connor, J.T., Zielinski, R.A., Bullock, J.H., Hower, J.C., Meeker, G.P., 2005. Characterization and Modes of Occurrence of Elements in Feed Coal and Coal Combustion Products from a Power Plant Utilizing Low-Sulfur Coal from the Powder River Basin, Wyoming (Scientific Investigations No. 2004–5271). U.S. Geological Survey, Reston, VA.

Burakov, A.E., Galunin, E.V., Burakova, I.V., Kucherova, A.E., Agarwal, S., Tkachev, A.G., Gupta, V.K., 2018. Adsorption of heavy metals on conventional and nanostructured materials for wastewater treatment purposes. Ecotoxicol. Environ. Saf. 148, 702–712.

Cen, L., Cheng, H., Liu, Q., Wang, S., Wang, X., 2022. Arsenic release from arsenopyrite weathering in acid mine drainage: Kinetics, transformation, and effect of biochar. Environ. Int. 170, 107558. https://doi.org/10.1016/j.envint.2022.107558

Chappaz, A., Glass, J.B., Lyons, T.W., 2018. Molybdenum, in: White, W.M. (Ed.), Encyclopedia of Geochemistry: A Comprehensive Reference Source on the Chemistry of the Earth, Encyclopedia of Earth Sciences Series. Springer International Publishing, Cham, pp. 947–950. https://doi.org/10.1007/978-3-319-39312-4_256

Cheng, K., Xu, X., Cui, L., Li, Y., Zheng, J., Wu, W., Sun, J., Pan, G., 2021. The role of soils in regulation of freshwater and coastal water quality. Philos. Trans. R. Soc. B Biol. Sci. 376, 20200176. https://doi.org/10.1098/rstb.2020.0176

Chmielewská, E., 2019. Chapter 4 - Natural zeolite: Alternative adsorbent in purification or post-treatment of waters, in: Mercurio, M., Sarkar, B., Langella, A. (Eds.), Modified Clay and Zeolite Nanocomposite Materials, Micro and Nano Technologies. Elsevier, pp. 87–112. https://doi.org/10.1016/B978-0-12-814617-0.00012-8

Colman, S.M., 1981. Rock-Weathering Rates as Functions of Time. Quat. Res. 15, 250–264. https://doi.org/10.1016/0033-5894(81)90029-6

Davison, W., 1993. Iron and manganese in lakes. Earth-Sci. Rev. 34, 119–163. https://doi.org/10.1016/0012-8252(93)90029-7

Dolton, G.L., Fox, J.E., Clayton, J.L., 1990. Petroleum geology of the Powder River basin, Wyoming and Montana (Open-file No. 88-450- P). U.S. Geological Survey. https://doi.org/10.3133/ofr88450P

Dos Santos, E.C., de Mendonça Silva, J.C., Duarte, H.A., 2016. Pyrite Oxidation Mechanism by Oxygen in Aqueous Medium. J. Phys. Chem. C 120, 2760–2768. https://doi.org/10.1021/acs.jpcc.5b10949

Dosseto, A., Turner, S.P., Chappell, J., 2008. The evolution of weathering profiles through time: New insights from uranium-series isotopes. Earth Planet. Sci. Lett. 274, 359–371. https://doi.org/10.1016/j.epsl.2008.07.050

Doulati Ardejani, F., Singh, R.N., Baafi, E., Porter, I., 2003. A Finite Element Model Simulate Groundwater Rebound Problems in Backfilled Open Cut Mines. Mine Water Environ. 22, 39–44. https://doi.org/10.1007/s102300300006

Dreher, G.B., Finkelman, R.B., 1992a. Selenium mobilization in a surface coal mine, Powder River Basin, Wyoming, U.S.A. Environ. Geol. Water Sci. 19, 155–167. https://doi.org/10.1007/BF01704083

Dreher, G.B., Finkelman, R.B., 1992b. Selenium mobilization in a surface coal mine, Powder River Basin, Wyoming, U.S.A. Environ. Geol. Water Sci. 19, 155–167. https://doi.org/10.1007/BF01704083

Drever, J.I., Clow, D.W., 1995. Weathering rates in catchments, in: Chemical Weathering Rates of Silicate Minerals. De Gruyter, pp. 463–483.

Dreybrodt, W., Lauckner, J., Zaihua, L., Svensson, U., Buhmann, D., 1996. The kinetics of the reaction CO2 + H2O → H+ + HCO3− as one of the rate limiting steps for the dissolution of calcite in the system H2O□CO2□CaCO3. Geochim. Cosmochim. Acta 60, 3375–3381. https://doi.org/10.1016/0016-7037(96)00181-0

Dunrud, C.R., Osterwald, F.W., 1978. Coal Mine Subsidence Near Sheridan, Wyoming. Environ. Eng. Geosci. xv, 175–190. https://doi.org/10.2113/gseegeosci.xv.2.175

Ellis, M.S., 2002. Quality of economically extractable coal beds in the Gillette coal field as compared with other Tertiary coal beds in the Powder River basin, Wyoming and Montana (USGS Numbered Series No. 2002–174), Open-File Report. U.S. Geological Survey, Reston, VA. https://doi.org/10.3133/ofr02174

Elrashidi, M.A., Adriano, D.C., Workman, S.M., Lindsay, W.L., 1987. Chemical Equilibria of Selenium in Soils: A Theoretical Development. Soil Sci. 144, 141–152.

Environmental Protection Agency, 1996. Sampling Ambient Water for Trace Metals at EPA Water Quality Criteria Levels Method 1669.

Fan, R., Qian, G., Li, Y., Short, M.D., Schumann, R.C., Chen, M., Smart, R.S.C., Gerson, A.R., 2022. Evolution of pyrite oxidation from a 10-year kinetic leach study: Implications for secondary mineralisation in acid mine drainage control. Chem. Geol. 588, 120653. https://doi.org/10.1016/j.chemgeo.2021.120653

Finkelman, R., 1987. The Inorganic Geochemistry of Coal: A Scanning Electron Microscopy View. Scanning Microsc. 2, 97–105.

Finkelman, R.B., Palmer, C.A., Wang, P., 2018. Quantification of the modes of occurrence of 42 elements in coal. Int. J. Coal Geol. 185, 138–160. https://doi.org/10.1016/j.coal.2017.09.005

Fischer, A.M., Van Hamme, J.D., Gardner, W.C., Fraser, L.H., 2022. Impacts from Topsoil Stockpile Height on Soil Geochemical Properties in Two Mining Operations in British Columbia: Implications for Restoration Practices. Mining 2, 315–329. https://doi.org/10.3390/mining2020017

Flores, R.M., 2004. Total Petroleum System and Assessment of Coalbed Gas in the Powder River Basin Province, Wyoming and Montana, U.S. Geological Survey Digital Data Series. USGS, Denver, CO.

Frascoli, F., Hudson-Edwards, K.A., 2018. Geochemistry, Mineralogy and Microbiology of Molybdenum in Mining-Affected Environments. Minerals 8, 42. https://doi.org/10.3390/min8020042

Futter, M.N., Klaminder, J., Lucas, R.W., Laudon, H., Köhler, S.J., 2012. Uncertainty in silicate mineral weathering rate estimates: source partitioning and policy implications. Environ. Res. Lett. 7, 024025. https://doi.org/10.1088/1748-9326/7/2/024025

Gaffney, J.W., White, K.N., Boult, S., 2008. Oxidation State and Size of Fe Controlled by Organic Matter in Natural Waters. Environ. Sci. Technol. 42, 3575–3581. https://doi.org/10.1021/es702880a

Gaillardet, J., Calmels, D., Romero-Mujalli, G., Zakharova, E., Hartmann, J., 2019. Global climate control on carbonate weathering intensity. Chem. Geol., Evolution of Carbonate and Karst Critical Zones 527, 118762. https://doi.org/10.1016/j.chemgeo.2018.05.009

Greber, N.D., Mäder, U., Nägler, T.F., 2015. Experimental dissolution of molybdenum-sulphides at low oxygen concentrations: A first-order approximation of late Archean atmospheric conditions. Earth Space Sci. 2, 173–180. https://doi.org/10.1002/2014EA000059

Hagmaier, J.L., 1971. Groundwater flow, hydrochemistry, and uranium deposition in the Powder River Basin, Wyoming (Doctoral dissertation). University of North Dakota.

Hassellöv, M., von der Kammer, F., 2008. Iron Oxides as Geochemical Nanovectors for Metal Transport in Soil-River Systems. Elements 4, 401–406. https://doi.org/10.2113/gselements.4.6.401

Hatje, V., Payne, T.E., Hill, D.M., McOrist, G., Birch, G.F., Szymczak, R., 2003. Kinetics of trace element uptake and release by particles in estuarine waters: effects of pH, salinity, and particle loading. Environ. Int. 29, 619–629. https://doi.org/10.1016/S0160-4120(03)00049-7

Healy, R.W., Rice, C.A., Bartos, T.T., McKinley, M.P., 2008. Infiltration from an impoundment for coal-bed natural gas, Powder River Basin, Wyoming: Evolution of water and sediment chemistry. Water Resour. Res. 44. https://doi.org/10.1029/2007WR006396

Hem, J.D., Cropper, W.H., 1962. Chemistry of Iron in Natural Water (USGS Numbered Series No. 1459), Geological Survey Water-Supply Paper. U.S. Geological Survey, Washington, U.S.

Hochella Jr, M.F., Lower, S.K., Maurice, P.A., Penn, R.L., Sahai, N., Sparks, D.L., Twining, B.S., 2008. Nanominerals, mineral nanoparticles, and Earth systems. Science 319, 1631–1635. https://doi.org/10.1126/science.1141134

Hochella Jr., M.F., Mogk, D.W., Ranville, J., Allen, I.C., Luther, G.W., Marr, L.C., McGrail, B.P., Murayama, M., Qafoku, N.P., Rosso, K.M., Sahai, N., Schroeder, P.A., Vikesland, P., Westerhoff, P., Yang, Y., 2019. Natural, incidental, and engineered nanomaterials and their impacts on the Earth system. Science 363. https://doi.org/10.1126/science.aau8299

Hochella, M.F., Lower, S.K., Maurice, P.A., Penn, R.L., Sahai, N., Sparks, D.L., Twining, B.S., 2008. Nanominerals, Mineral Nanoparticles, and Earth Systems. Science 319, 1631–1635. https://doi.org/10.1126/science.1141134

Hochella, M.F., Mogk, D.W., Ranville, J., Allen, I.C., Luther, G.W., Marr, L.C., McGrail, B.P., Murayama, M., Qafoku, N.P., Rosso, K.M., Sahai, N., Schroeder, P.A., Vikesland, P., Westerhoff, P., Yang, Y., 2019. Natural, incidental, and engineered nanomaterials and their impacts on the Earth system. Science 363, eaau8299. https://doi.org/10.1126/science.aau8299

Holub, M., Balintova, M., Pavlikova, P., Palascakova, L., 2013. Study of sorption properties of zeolite in acidic conditions in dependence on particle size. Ital. Assoc. Chem. Eng. 32, 559–564.

Hu, G., Dam-Johansen, K., Wedel, S., Hansen, J.P., 2006. Decomposition and oxidation of pyrite. Prog. Energy Combust. Sci. 32, 295–314. https://doi.org/10.1016/j.pecs.2005.11.004

Huggins, F.E., Huffman, G.P., Lin, M.C., 1983. Observations on low-temperature oxidation of minerals in bituminous coals. Int. J. Coal Geol. 3, 157–182. https://doi.org/10.1016/0166-5162(83)90008-3

Jiang, N., Shang, R., Heijman, S.G.J., Rietveld, L.C., 2018. High-silica zeolites for adsorption of organic micro-pollutants in water treatment: A review. Water Res. 144, 145–161. https://doi.org/10.1016/j.watres.2018.07.017

Johnson, A.C., Romaniello, S.J., Reinhard, C.T., Gregory, D.D., Garcia-Robledo, E., Revsbech, N.P., Canfield, D.E., Lyons, T.W., Anbar, A.D., 2019. Experimental determination of pyrite and molybdenite oxidation kinetics at nanomolar oxygen concentrations. Geochim. Cosmochim. Acta 249, 160–172. https://doi.org/10.1016/j.gca.2019.01.022

Journet, E., Desboeufs, K.V., Caquineau, S., Colin, J.-L., 2008. Mineralogy as a critical factor of dust iron solubility. Geophys. Res. Lett. 35. https://doi.org/10.1029/2007GL031589

Jun, Y.-S., Lee, B., Waychunas, G.A., 2010. In Situ Observations of Nanoparticle Early Development Kinetics at Mineral−Water Interfaces. Environ. Sci. Technol. 44, 8182–8189. https://doi.org/10.1021/es101491e

Karfakis, M.G., Topuz, E., 1991. Post mining subsidence abatements in Wyoming abandoned coal mines. Min. Sci. Technol. 12, 215–231. https://doi.org/10.1016/0167-9031(91)91137-7

Kolker, A., Mroczkowski, S.J., Palmer, C.A., Dennen, K.O., Finkelman, R.B., Bullock, J.H., 2002. Toxic Substances From Coal Combustion- A Comprehensive Assessment, Phase II: Element Modes of Occurrence for the Ohio 5/6/7, Wyodak and North Dakota Coal Samples. Final Technical Report (USGS Numbered Series No. 2002–224), Open-File Report. U.S. Geological Survey.

Langman, J.B., Blowes, D.W., Veeramani, H., Wilson, D., Smith, L., Sego, D.C., Paktunc, D., 2015. The mineral and aqueous phase evolution of sulfur and nickel with weathering of pyrrhotite in a low sulfide, granitic waste rock. Chem. Geol. 401, 169–179. https://doi.org/10.1016/j.chemgeo.2015.02.024

Lapakko, K.A., 2003. Developments in humidity-cell tests and their application [WWW Document]. ResearchGate. URL https://www.researchgate.net/publication/284026337_Developments_in_humidity-cell_tests_and_their_application (accessed 5.3.23).

Lapakko, K.A., White, W.W., 2000. Modification of the ASTM 5744-96 Kinetic Test, in: Proceedings from the 5th International Conference on Acid Rock Drainage. Presented at the International Conference on Acid Rock Drainage, Littleton, Colorado.

Lasaga, A.C., 1984. Chemical kinetics of water-rock interactions. J. Geophys. Res. Solid Earth. https://doi.org/10.1029/JB089iB06p04009Li

Lebedev, A.L., 2015. Kinetics of gypsum dissolution in water. Geochem. Int. 53, 811–824. https://doi.org/10.1134/S0016702915070058

Lebedeva, M. i., Brantley, S. l., 2020. Relating the depth of the water table to depth of weathering. Earth Surf. Process. Landf. n/a. https://doi.org/10.1002/esp.4873

Lee, R.W., 1980. Geochemistry of water in the Fort Union Formation of the northern Powder River basin, southeastern Montana (USGS Numbered Series No. 80–336), Geochemistry of water in the Fort Union Formation of the northern Powder River basin, southeastern Montana, Open-File Report. U.S. Geological Survey, https://doi.org/10.3133/ofr80336

Lehmann, N., Lantuit, H., Böttcher, M.E., Hartmann, J., Eulenburg, A., Thomas, H., 2022. Alkalinity generation from carbonate weathering in a silicate-dominated headwater catchment at Iskorasfjellet, northern Norway. Biogeosciences Discuss. 1–39. https://doi.org/10.5194/bg-2022-205

Li, W., Liu, X.-M., Hu, Yan, Teng, F.-Z., Hu, Yongfeng, 2021. Potassium isotopic fractionation during clay adsorption. Geochim. Cosmochim. Acta 304, 160–177. https://doi.org/10.1016/j.gca.2021.04.027

Liang, L., Morgan, J.J., 1990. Chemical aspects of iron oxide coagulation in water: Laboratory studies and implications for natural systems. Aquat. Sci. 52, 32–55. https://doi.org/10.1007/BF00878240

Lorenz, J.C., Nadon, G.C., 2002. Braided-River Deposits in A Muddy Depositional Setting: The Molina Member of the Wasatch Formation (Paleogene), West-Central Colorado, U.S.A. J. Sediment. Res. 72, 376–385. https://doi.org/10.1306/100801720376

Malmström, M., Banwart, S., 1997. Biotite dissolution at 25°C: The pH dependence of dissolution rate and stoichiometry. Geochim. Cosmochim. Acta 61, 2779–2799. https://doi.org/10.1016/S0016-7037(97)00093-8

Malmström, M.E., Destouni, G., Banwart, S.A., Strömberg, B.H.E., 2000. Resolving the Scale-Dependence of Mineral Weathering Rates. Environ. Sci. Technol. 34, 1375–1378. https://doi.org/10.1021/es990682u

Margeta, K., Zabukovec, N., Siljeg, M., Farkas, A., 2013. Natural Zeolites in Water Treatment—How Effective is Their Use, in: Elshorbagy, W. (Ed.), Water Treatment. InTech.

McClurg, J.E., 1988. Peat forming wetlands and the thick Powder River Basin coals. Presented at the Wyoming Geological Association 39th Annual Field Conference, Wyoming Geological Association, pp. 229–236.

Milligan, C., Reddy, K., 2007. Monitoring of Groundwater Contamination by Trace Elements from CBNG Disposal Ponds Across the Powder River Basin, Wyoming. J. Am. Soc. Min. Reclam. 2007. https://doi.org/10.21000/JASMR07010520

Moore, T.A., 1991. The effects of clastic sedimentation on organic facies development within a Tertiary subbituminous coal bed, Powder River Basin, Montana, U.S.A. Int. J. Coal Geol. 18, 187–209. https://doi.org/10.1016/0166-5162(91)90050-S

Motsi, T., Rowson, N.A., Simmons, M.J.H., 2009. Adsorption of heavy metals from acid mine drainage by natural zeolite. Int. J. Miner. Process. 92, 42–48. https://doi.org/10.1016/j.minpro.2009.02.005

Naderian, A.R., Williams, D.J., Clark, I.H., 1996. Numerical modelling of settlements in back-filled open-cut coal mines. Int. J. Surf. Min. Reclam. Environ. 10, 25–29. https://doi.org/10.1080/09208119608964791

Navrotsky, A., Mazeina, L., Majzlan, J., 2008. Size-Driven Structural and Thermodynamic Complexity in Iron Oxides. Science 319, 1635–1638. https://doi.org/10.1126/science.1148614

Palmer, C.A., Kolker, A., Finkelman, R.B., Kolb, K.C., Mroozkowski, S.J., Crowley, S.S., Belkin, H.E., Bullock, J., Motooka, J.M., 1997. Trace Elements in Coal - Modes of Ocurrence Analysis. (No. DOE/PC/95156-04). Minerals Management Service, Reston, VA (United States). https://doi.org/10.2172/644624

Palmer, C.A., Mroozkowski, S.J., Kolker, A., Finkelman, R.B., Bullock, J.H., 2001. Chemical analysis and modes of occurrence of selected trace elements in a Powder River basin coal and its corresponding simulated cleaned coal (USGS Numbered Series No. 2000–323), Open-File Report. U.S. Geological Survey.

Pandová, I., Panda, A., Valíček, J., Harničárová, M., Kušnerová, M., Palková, Z., 2018. Use of sorption of copper cations by clinoptilolite for wastewater treatment. Int. J. Environ. Res. Public. Health 15, 1364. https://doi.org/10.3390/ijerph15071364

Paydary, P., Schellenger, A.E.P., Teli, M., Jaisi, D.P., Onnis-Hayden, A., Larese-Casanova, P., 2021. Chemical oxidation of selenite to selenate: Evaluation of reactive oxygen species and O transfer pathways. Chem. Geol. 575, 120229. https://doi.org/10.1016/j.chemgeo.2021.120229

Peabody Energy, 2022. North Antelope Rochelle Mine (Technical report No. SK-1300). Saint Louis, Missouri.

Perret, D., Gaillard, J.-F., Dominik, J., Atteia, O., 2000. The Diversity of Natural Hydrous Iron Oxides. Environ. Sci. Technol. 34, 3540–3546. https://doi.org/10.1021/es0000089

Plathe, K.L., von der Kammer, F., Hassellöv, M., Moore, J.N., Murayama, M., Hofmann, T., Hochella Jr., M.F., 2013. The role of nanominerals and mineral nanoparticles in the transport of toxic trace metals: Field-flow fractionation and analytical TEM analyses after nanoparticle isolation and density separation. Geochim. Cosmochim. Acta 102, 213–225. https://doi.org/10.1016/j.gca.2012.10.029

Pocknall, D.T., 1987. Paleoenvironments and age of the Wasatch Formation (Eocene), Powder River basin, Wyoming. PALAIOS 2, 386–375. https://doi.org/10.2307/3514762

Possemiers, M., Huysmans, M., Anibas, C., Batelaan, O., Van Steenwinkel, J., 2016. Reactive transport modeling of redox processes to assess Fe(OH)3 precipitation around aquifer thermal energy storage wells in phreatic aquifers. Environ. Earth Sci. 75, 648. https://doi.org/10.1007/s12665-016-5398-7

Reddy, K.J., Zhang, Z., Vance, G.F., 1995. Selenite and Selenate Determination in Surface Coal Mine Backfill Ground Water. https://doi.org/10.21000/jasmr95010237

Reed, S.M., Singh, R.N., 1986. Groundwater recovery problems associated with opencast mine backfills in the United Kingdom. Int. J. Mine Water 5, 47–73. https://doi.org/10.1007/BF02551534

Rice, C.A., Flores, R.M., Stricker, G.D., Ellis, M.S., 2008. Chemical and stable isotopic evidence for water/rock interaction and biogenic origin of coalbed methane, Fort Union Formation, Powder River Basin, Wyoming and Montana U.S.A. Int. J. Coal Geol., Microbes, Methanogenesis, and Microbial Gas in Coal 76, 76–85. https://doi.org/10.1016/j.coal.2008.05.002

Roehler, H.W., 1987. Geologic Investigations of the Vermillion Creek Coal Bed in the Eocene Niland Tongue of the Wasatch Formation, Sweetwater County, Wyoming. U.S. Geological Survey.

Salmon, S.U., Malmström, M.E., 2006. Quantification of mineral dissolution rates and applicability of rate laws: Laboratory studies of mill tailings. Appl. Geochem. 21, 269–288. https://doi.org/10.1016/j.apgeochem.2005.09.014

Schwertmann, U., 1991. Solubility and dissolution of iron oxides. Plant Soil 130, 1–25. https://doi.org/10.1007/BF00011851

See, R.B., Reddy, K.J., Vance, G.F., Fadlelmawla, A.A., Blaylock, M.J., 1995. Geochemical processes and the effects of natural organic solutes on the solubility of selenium in coal-mine backfill samples from the Powder River basin, Wyoming (USGS Numbered Series No. 95–4200), Geochemical processes and the effects of natural organic solutes on the solubility of selenium in coal-mine backfill samples from the Powder River basin, Wyoming, Water-Resources Investigations Report. U.S. Geological Survey. https://doi.org/10.3133/wri954200

Sharma, V., Filip, J., Zboril, R., S. Varma, R., 2015. Natural inorganic nanoparticles – formation, fate, and toxicity in the environment. Chem. Soc. Rev. 44, 8410–8423. https://doi.org/10.1039/C5CS00236B

Silva, J.C.M., Santos, E.C. dos, Heine, T., Abreu, H.A.D., Duarte, H.A., 2017. Oxidation Mechanism of Arsenopyrite in the Presence of Water [WWW Document]. ACS Publ. https://doi.org/10.1021/acs.jpcc.7b09706

Skorina, T., Allanore, A., 2015. Aqueous alteration of potassium-bearing aluminosilicate minerals: from mechanism to processing. Green Chem. 17, 2123–2136. https://doi.org/10.1039/C4GC02084G

Slagle, S.E., Lewis, B., Lee, R., 1985. Ground-water resources and potential hydrologic effects of surface coal mining in the northern Powder River basin, southeastern Montana (USGS Numbered Series No. 2239), Water Supply Paper. U.S. Geological Survey. https://doi.org/10.3133/wsp2239

Sparks, D.L., 1991. Chemical Kinetics and Mass Transfer Processes in Soils and Soil Constituents, in: Bear, J., Corapcioglu, M.Y. (Eds.), Transport Processes in Porous Media, NATO ASI Series. Springer Netherlands, Dordrecht, pp. 583–637. https://doi.org/10.1007/978-94-011-3628-0_12

St-Arnault, M., Vriens, B., Blaskovich, R., Aranda, C., Klein, B., Ulrich Mayer, K., Beckie, R.D., 2020a. Geochemical and mineralogical assessment of reactivity in a full-scale heterogeneous waste-rock pile. Miner. Eng. 145, 106089. https://doi.org/10.1016/j.mineng.2019.106089

St-Arnault, M., Vriens, B., Blaskovich, R., Aranda, C., Klein, B., Ulrich Mayer, K., Beckie, R.D., 2020b. Geochemical and mineralogical assessment of reactivity in a full-scale heterogeneous waste-rock pile. Miner. Eng. 145, 106089. https://doi.org/10.1016/j.mineng.2019.106089

St-Arnault, M., Vriens, B., Klein, B., Mayer, K.U., Beckie, R.D., 2019. Mineralogical controls on drainage quality during the weathering of waste rock. Appl. Geochem. 108, 104376. https://doi.org/10.1016/j.apgeochem.2019.104376

Stillings, L.L., 2017. Selenium (USGS Numbered Series No. 1802- Q), Selenium, Professional Paper. U.S. Geological Survey, Reston, VA. https://doi.org/10.3133/pp1802Q

Stockwell, J., Smith, L., Jambor, J.L., Beckie, R., 2006. The relationship between fluid flow and mineral weathering in heterogeneous unsaturated porous media: A physical and geochemical characterization of a waste-rock pile. Appl. Geochem. 21, 1347–1361. https://doi.org/10.1016/j.apgeochem.2006.03.015

Stoeppler, M., 1992. Chapter 8 - Cadmium, in: Stoeppler, M. (Ed.), Techniques and Instrumentation in Analytical Chemistry, Hazardous Metals in the Environment. Elsevier, pp. 177–230. https://doi.org/10.1016/S0167-9244(08)70107-0

Stylianou, M.A., Hadjiconstantinou, M.P., Inglezakis, V.J., Moustakas, K.G., Loizidou, M.D., 2007. Use of natural clinoptilolite for the removal of lead, copper and zinc in fixed bed column - ScienceDirect. J. Hazard. Mater. 143, 575–581.

Sun, H., Chen, M., Zou, L., Shu, R., Ruan, R., 2015. Study of the kinetics of pyrite oxidation under controlled redox potential. Hydrometallurgy 155, 13–19. https://doi.org/10.1016/j.hydromet.2015.04.003

Sun, Q., Zhou, N., Quan, K., Chen, Y., 2017. Stability analysis and control of embankment with solid backfill coal mining. Min. Technol. 126, 104–112. https://doi.org/10.1080/14749009.2017.1287459

Szekeres, M., Tombácz, E., 2012. Surface charge characterization of metal oxides by potentiometric acid–base titration, revisited theory and experiment. Colloids Surf. Physicochem. Eng. Asp. 414, 302–313. https://doi.org/10.1016/j.colsurfa.2012.08.027

Tabelin, C.B., Corpuz, R.D., Igarashi, T., Villacorte-Tabelin, M., Alorro, R.D., Yoo, K., Raval, S., Ito, M., Hiroyoshi, N., 2020. Acid mine drainage formation and arsenic mobility under strongly acidic conditions: Importance of soluble phases, iron oxyhydroxides/oxides and nature of oxidation layer on pyrite. J. Hazard. Mater. 399, 122844. https://doi.org/10.1016/j.jhazmat.2020.122844

Torres, R., Segura-Bailón, B., Lapidus, G.T., 2018. Effect of temperature on copper, iron and lead leaching from e-waste using citrate solutions. Waste Manag. 71, 420–425. https://doi.org/10.1016/j.wasman.2017.10.029

United States Geological Survey, 2006. Chapter A4. Collection of water samples (USGS Numbered Series No. 09-A4), Chapter A4. Collection of water samples, Techniques of Water-Resources Investigations. U.S. Geological Survey, Reston, VA. https://doi.org/10.3133/twri09A4

Vance, G.F., See, R.B., Reddy, K.J., 1998. Selenite Sorption by Coal Mine Backfill Materials in the Presence of Organic Solutes, in: Frankenberger, W.T., Engberg, R.A. (Eds.), Environmental Chemistry of Selenium. Marcel Dekker, Inc., New York, pp. 259–280. https://doi.org/10.1201/9781482269949-18

Vriens, B., Skierszkan, E.K., St-Arnault, M., Salzsauler, K., Aranda, C., Mayer, K.U., Beckie, R.D., 2019a. Mobilization of Metal(oid) Oxyanions through Circumneutral Mine Waste-Rock Drainage. ACS Omega 4, 10205–10215. https://doi.org/10.1021/acsomega.9b01270

Vriens, B., Smith, L., Mayer, K.U., Beckie, R.D., 2019b. Poregas distributions in waste-rock piles affected by climate seasonality and physicochemical heterogeneity. Appl. Geochem. 100, 305–315. https://doi.org/10.1016/j.apgeochem.2018.12.009

Wang, H., Jiang, R., Wang, B., Yao, S., 2021. The Effect of Gypsum on the Fixation of Selenium in the Iron/Calcium-Selenium Coprecipitation Process. Bull. Environ. Contam. Toxicol. 106, 121–125. https://doi.org/10.1007/s00128-020-02881-2

Wang, L., Reddy, K.J., Munn, L.C., 1994. Geochemical modeling for predicting potential solid phases controlling the dissolved molybdenum in coal overburden, Powder River Basin, WY, U.S.A. Appl. Geochem. 9, 37–43. https://doi.org/10.1016/0883-2927(94)90050-7

Wang, S., Peng, Y., 2010. Natural zeolites as effective adsorbents in water and wastewater treatment - ScienceDirect. Chem. Eng. J. 156, 11–24.

Wang, Z., Li, R., Cui, L., Fu, H., Lin, J., Chen, J., 2018. Characterization and acid-mobilization study for typical iron-bearing clay mineral. J. Environ. Sci. 71, 222–232. https://doi.org/10.1016/j.jes.2018.04.012

Waychunas, G.A., Kim, C.S., Banfield, J.F., 2005. Nanoparticulate iron oxide minerals in soils and sediments: Unique properties and contaminant scavenging mechanisms. J. Nanoparticle Res. 7, 409–433. https://doi.org/10.1007/s11051-005-6931-x

Weber, F.-A., Hofacker, A.F., Voegelin, A., Kretzschmar, R., 2010. Temperature Dependence and Coupling of Iron and Arsenic Reduction and Release during Flooding of a Contaminated Soil. Environ. Sci. Technol. 44, 116–122. https://doi.org/10.1021/es902100h

White, A.F., Blum, A.E., Schulz, M.S., Bullen, T.D., Harden, J.W., Peterson, M.L., 1996. Chemical weathering rates of a soil chronosequence on granitic alluvium: I. Quantification of mineralogical and surface area changes and calculation of primary silicate reaction rates. Geochim. Cosmochim. Acta 60, 2533–2550. https://doi.org/10.1016/0016-7037(96)00106-8

White, A.F., Brantley, S.L., 1995. Chemical weathering rates of silicate minerals: an overview, in: Chemical Weathering Rates of Silicate Minerals. De Gruyter, pp. 1–22. https://doi.org/10.1515/9781501509650-003

Williamson, M.A., Rimstidt, J.D., 1994a. The kinetics and electrochemical rate-determining step of aqueous pyrite oxidation. Geochim. Cosmochim. Acta 58, 5443–5454. https://doi.org/10.1016/0016-7037(94)90241-0

Williamson, M.A., Rimstidt, J.D., 1994b. The kinetics and electrochemical rate-determining step of aqueous pyrite oxidation. Geochim. Cosmochim. Acta 58, 5443–5454. https://doi.org/10.1016/0016-7037(94)90241-0

Wunderly, M.D., Blowes, D.W., Frind, E.O., Ptacek, C.J., 1996. Sulfide mineral oxidation and subsequent reactive transport of oxidation products in mine tailings impoundments: A numerical model. Water Resour. Res. 32, 3173–3187. https://doi.org/10.1029/96WR02105

Wyoming State Engineer's Office, 1995. Fort Union Formation Aquifer Monitoring Plan and Preliminary Aquifer Management Plan. Wyoming Water Development Commission, Gillette, Wyoming.

Yoo, K., Mudd, S.M., 2008. Discrepancy between mineral residence time and soil age: Implications for the interpretation of chemical weathering rates | Geology | GeoScienceWorld [WWW Document]. Geosci. World. URL https://pubs.geoscienceworld.org/gsa/geology/article-abstract/36/1/35/129993/Discrepancy-between-mineral-residence-time-and?redirectedFrom=fulltext (accessed 5.3.23).

Yudovich, Ya.E., Ketris, M.P., 2006. Selenium in coal: A review. Int. J. Coal Geol. 67, 112–126. https://doi.org/10.1016/j.coal.2005.09.003

Yudovich, Y.E., Ketris, M.P., 2006. Selenium in coal: A review. Int. J. Coal Geol. 67, 112–126. https://doi.org/10.1016/j.coal.2005.09.003

Yuretich, R.F., Hickey, L.J., Gregson, B.P., Hsia, Y.L., 1984. Lacustrine Deposits in the Paleocene Fort Union Formation, Northern Bighorn Basin, Montana. J. Sediment. Res. 54, 836–852. https://doi.org/10.1306/212F8512-2B24-11D7-8648000102C1865D

Zhang, J., Li, M., Taheri, A., Zhang, W., Wu, Z., Song, W., 2019. Properties and Application of Backfill Materials in Coal Mines in China. Minerals 9, 53. https://doi.org/10.3390/min9010053

Supplemental Data

Supplementary data file: https://www.mdpi.com/2076-3263/14/1/4#app1-geosciences-14-00004

Publications at the Time of Report Completion

Attached: Martin, J.; Langman, J.B. Leachate Experiments to Evaluate Weathering of Waste Rock for Backfill Aquifers in Restored Coal Mine Pits, Powder River Basin, USA. *Geosciences* **2024**, *14*, 4. https://doi.org/10.3390/geosciences14010004